Canopy structure, topography and weather are equally important drivers of small-scale snow cover dynamics in sub-alpine forests

Giulia Mazzotti[1,2], Clare Webster[1,3], Louis Quéno[1], Bertrand Cluzet[1], Tobias Jonas[1]

[1]WSL Institute for Snow and Avalanche Research SLF, 7260 Davos Dorf, Switzerland
[2]Univ. Grenoble Alpes, Université de Toulouse, Météo-France, CNRS, CNRM, Centre d'Études de la Neige, 38100 St. Martin d'Hères, France
[3]Department of Geosciences, University of Oslo, 0316 Oslo, Norway

Correspondence to: Giulia Mazzotti (giulia.mazzotti@slf.ch)

Abstract. In mountain regions, forests that overlap with seasonal snow mostly reside in complex terrain. Due to persisting major observational challenges in these environments, the combined impact of forest structure and topography on seasonal snow cover dynamics is still poorly understood. Recent advances in forest snow process representation and increasing availability of detailed canopy structure datasets, however, now allow for hyper-resolution (<5 m) snow model simulations capable of resolving tree-scale processes. These can shed light on the complex process interactions that govern forest snow dynamics. We present multi-year simulations at 2 m resolution obtained with FSM2, a mass- and energy-balance based forest snow model specifically developed and validated for meter-scale applications. We simulate a ~–3 km^2 model domain encompassing forested slopes of a sub-alpine valley in the Eastern Swiss Alps and six snow seasons. Simulations thus span a wide range of canopy structures, terrain characteristics, and meteorological conditions. We analyse spatial and temporal variations in forest snow energy balance partitioning, aiming to quantify and understand the contribution of individual energy exchange processes at different locations and times. Our results suggest that snow cover evolution is equally affected by canopy structure, terrain characteristics and meteorological conditions. We show that the interaction of these three factors can lead to snow accumulation and ablation patterns that vary between years. We further identify higher snow distribution variability and complexity in slopes that receive solar radiation early in winter. Our process-level insights corroborate and complement existing empirical findings that are largely based on snow distribution datasets only. Hyper-resolution simulations as presented here thus help to better understand how snowpacks and ecohydrological regimes in sub-alpine regions may evolve due to forest disturbances and a warming climate. They could further support the development of process-based sub-grid forest snow cover parametrizations or tiling approaches for coarse-resolution modelling applications.

1 Introduction

The presence of snow in the sub-alpine forest ecoregion of the European Alps, and other mountain ranges across the Northern Hemisphere, means large areas of seasonal snow cover overlap with both forests and complex topography. Snow accumulation and ablation processes are known to be controlled by the structure of the forest cover (Mazzotti et al., 2019a), topographic

characteristics (Broxton et al., 2020; Safa et al., 2021; Schirmer and Pomeroy, 2020), as well as how these physiographic factors interact with local climate and weather patterns (Lundquist et al., 2013; Seyednasrollah and Kumar, 2019; Pflug and Lundquist, 2020). Consequently, snow cover dynamics in sub-alpine forest are subject to strong complexity and variability down to small spatial and temporal scales. A thorough understanding of the controlling factors is important because snow cover dynamics affect eco-hydrological regimes (e.g. Barnhart et al., 2016; Manning et al., 2022), microclimate and habitat characteristics (e.g. Niittynen et al., 2020), as well as land surface energy exchange (e.g. Webster and Jonas, 2018; Manninen and Jääskeläinen, 2018). Today, snow cover regimes are changing due to climate warming (Mote et al., 2018; Marty et al., 2017; Notarnicola, 2020; Bormann et al., 2018), and forest structure is being altered by manmade and natural disturbances (Bebi et al., 2017; Seidl et al., 2017; Goeking and Tarboton, 2020). In view of these changes, understanding forest-snow dynamics can inform adequate management strategies - particularly in regions where downstream water supply is dependent on snow resources from forested headwaters (Sturm et al., 2017; Siirila-Woodburn et al., 2021). However, it remains unclear if and how the response of snow cover dynamics to environmental change will depend on where this snow is located within the heterogeneous landscape.

Canopy structural controls on individual forest processes have been widely addressed in both experimental and modelling studies. Interception of snow by the canopy (Moeser et al., 2015; Roth and Nolin, 2019), transmission of shortwave, and enhancement of longwave radiation (Malle et al., 2019; Mazzotti et al., 2019b; Webster et al., 2016; Lawler and Link, 2011), have received particular attention due to the strong spatial variability of these processes induced by tree-scale canopy structural heterogeneity. Existing research has, however, focused on flat sites to single out the effect of canopy structure. Only few studies have considered how the combination of forest and topography alter accumulation and ablation processes under forest relative to clearings. Ellis et al. (2011) presented measurements from a Canadian site, including short- and longwave irradiances and snow depth under the canopy and in clearings on different slopes and aspects, and showed that the presence of forest delayed snowmelt relative to open areas more strongly on south-exposed slopes than on north-exposed ones. In a modelling study, Strasser et al. (2011) found that forest cover diminished aspect-dependent differences in snow cover dynamics compared to openings, and further noted that forest effects differed between years with varying meteorological conditions. Neither of these studies did, however, consider fine-scale canopy structure in detail, and no study that specifically addresses inter-annual consistency of fine-scale forest snow distribution patterns exists to our knowledge.

In recent years, the increased availability of LiDAR-derived snow depth distribution datasets has enabled a new approach to analysing forest snow cover dynamics. Multiple studies have attempted to establish relationships between snow, canopy, and terrain descriptors based on such datasets (Zheng et al., 2019; Mazzotti et al., 2019a; Currier and Lundquist, 2018). Broxton et al. (2020) used maps of snow water equivalent (SWE) and time series of snow depth transect measurements to analyse the combined impact of forest density and topographic location on snow water equivalent in a semi-arid climate. Safa et al. (2021) applied machine learning to identify the factors that determine snow disappearance in different forest and topographic settings based on snow depth maps covering four US sites with variable climate characteristics. Recently, Koutantou et al. (2022) presented a time series of Uncrewed Aerial Vehicle (UAV) borne LiDAR datasets to compare the evolution of snow depth

distribution patterns on opposed slopes in an Alpine valley. All these studies were limited to process inferences as snow distribution datasets only reflect the combined impact of various forest snow processes.

Instead of relying on snow data alone, understanding process interactions can be advanced through sophisticated process-based models. In absence of observational data, or for predictive purposes, models are commonly used as a best estimate of reality (Wood et al., 2011; Wrzesien et al., 2022). In forest snow research, the use of hyper-resolution models that resolve tree-scale processes is gaining popularity in applications that require the small-scale variability of these processes to be adequately represented (Harpold et al., 2020). To our knowledge, two models developed specifically for this purpose exist to date: SnowPALM - Snow Physics and LiDAR Mapping (Broxton et al., 2015) and FSM2 - Flexible Snow Model (Mazzotti et al., 2020a, b). They evolved independent of each other but follow similar principles: At every modelled location, the computation of forest snow processes considers the specific canopy structure both directly overhead and in the surroundings of the location of interest. This approach acknowledges the fact that different characteristics of the canopy are relevant for different processes. For instance, it allows for a model grid cell located in a forest gap to be unaffected by interception of snow in the canopy (due to lack of overhead canopy), but still experience reduced insolation and wind speeds (due to sheltering by the surrounding canopy); whereas a grid cell underneath a tree at the canopy edge may be affected by both interception and direct insolation. Such a representation requires explicit canopy structure descriptors to be derived from canopy structure data at equally high spatial resolution.

The benefit of hyper-resolution canopy representations relative to traditional approaches that rely on bulk canopy descriptors like Leaf Area Index (LAI) and average canopy height only has been demonstrated for both FSM2 and SnowPALM. Both models have been shown to effectively capture detailed snow depth distribution patterns when compared to manual and LiDAR-derived measurements (Broxton et al., 2015; Mazzotti et al., 2020b). In addition, FSM2 has also been validated at the level of individual processes by comparing modelled sub-canopy incoming short- and longwave radiation, air and snow surface temperature, and wind speed, against spatially and temporally resolved observational datasets (Mazzotti et al., 2020a). To our knowledge, such a validation approach is unprecedented, revealing remarkable improvements in resolving canopy-mediated processes at a high spatial and temporal resolutions.

Their ability to accurately capture process variability has made hyper-resolution forest snow models attractive research tools. Impact studies have used SnowPALM to analyse the effect of forest disturbance on snow water resources under varying meteorological conditions (Moeser et al., 2020), and to assess forest thinning strategies (Krogh et al., 2020). Hyper-resolution models also provide an approximation of processes that are not resolved in coarser resolution models and can thus inform the development of sub-grid parametrizations of these processes. As such, both SnowPALM (Broxton et al., 2021) and FSM2 (Mazzotti et al., 2021) have been used to derive recommendations for modelling forest snow processes at coarser resolutions, and there is still great potential to further exploit these models for scientific purposes.

In this study, we used hyper-resolution modelling to explore the spatio-temporal dynamics of individual forest snow processes and their effect on snow cover evolution in forested complex terrain under varying meteorological conditions. We applied~~y~~ FSM2 to a sub-alpine valley and across multiple winters to assess the interplay of canopy structure, topography, and

meteorology. Our work builds on Koutantou et al. (2022), who observed considerable differences in snow distribution dynamics between their sites located on south- and north-exposed forested slopes over the course of one snow season. The authors hypothesized that weaker correlations between snow depth and canopy cover at the south-exposed than at the north-exposed slope were due to differences in the shortwave irradiance regimes at the two locations but could not fully demonstrate this based on their observational data of snow depth alone. The modelling approach used here ~~allows~~ allowed us to overcome the limitations of their study by leveraging the capabilities of FSM2 to accurately represent both snow distribution and the spatio-temporal dynamics of the underlying processes. Based on the respective simulations, we ~~will~~ analysed individual processes and their interactions over larger spatial and temporal extents than previously possible, where equivalent observational datasets are inexistent. Our goals ~~are~~ were (1) to characterize spatial patterns of snow cover dynamics and the underlying processes in such a sub-alpine environment; (2) to detect connectivity between snow patterns and patterns of underlying processes; and (3) to assess their temporal consistency throughout the season and between different years. By contributing to the improved understanding of these dynamics, we hope to facilitate the development of approaches to treat sub-grid variability in coarser-resolution models, and to help expand our capabilities to assess the impact of environmental change on ecohydrological processes.

2 Methods

2.1 Study area

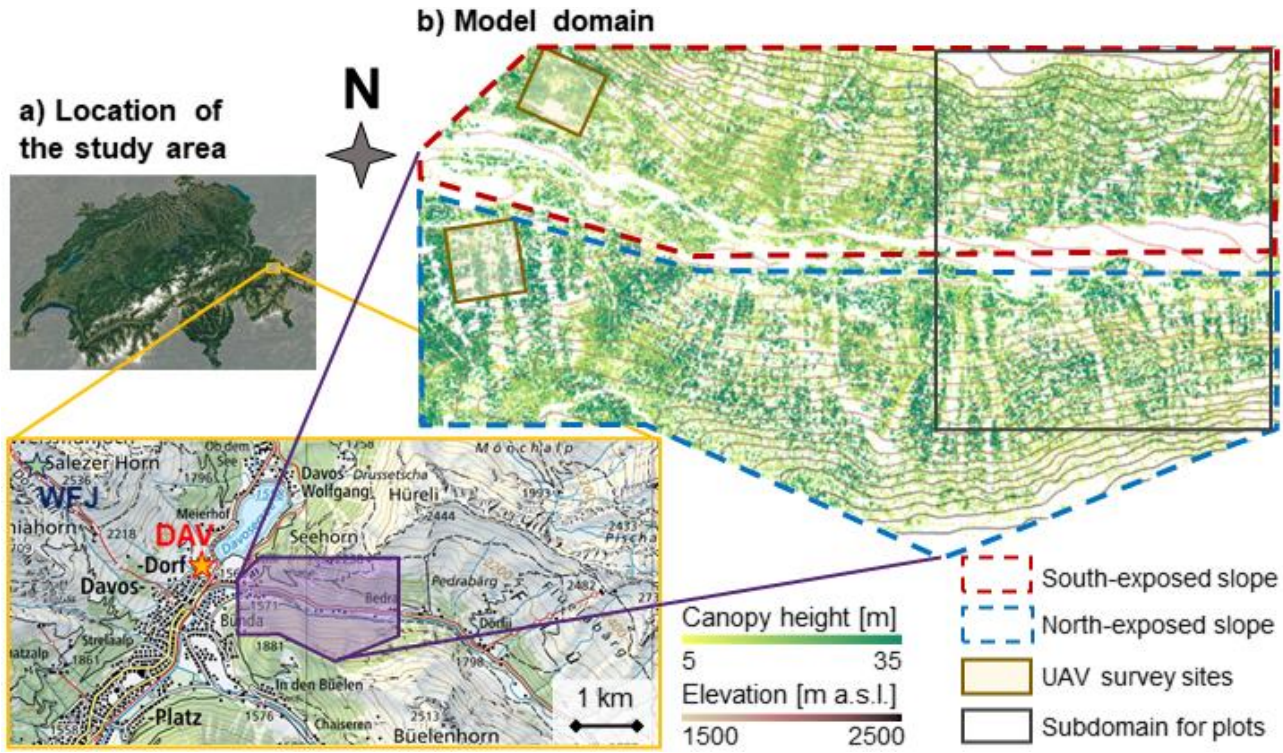

Figure 1: Overview of the study area: (a) Location of the model domain within Switzerland and on the topographic map of the Davos area (source: swisstopo), including locations of the automatic weather stations DAV and WFJ; (b) Canopy height model and contour lines (equidistance: 50m), including locations of the sites from Koutantou et al. (2022) and of the subdomain shown in Figures 5 and 7-9.

We focused our modelling in a domain situated in the Flüela valley near Davos (Figure 1) in the Eastern Swiss Alps. The climate is inner-alpine with an average wintertime (DJF) air temperature of -4.2 °C and 450 mm yearly snowfall sum (Davos station, MeteoSwiss, norm period 1991-2020; www.meteoschweiz.ch). The model domain is contained in a 2.5 x 1.5 km area at the entry of the valley, which consists of two opposite (south- and a north-facing) slopes. Both slopes extend over 500 m elevation span from the valley bottom at 1570 m a.s.l. to the tree line around 2100 m. Maps of the topographic characteristics of the model domain (elevation, slope, and aspect) are included in the Supplementary Material (Figure S1.1).

The forest comprises needleleaf species, predominantly Norway spruce (evergreen) with some individual larches (deciduous), which is typical of this sub-alpine forest ecoregion. Understory vegetation is short, mainly consisting of blueberry bushes and grasses. Trees range from new- to old growths with maximum heights of 35 m, and forest structure includes both dense stands and gaps of varied sizes. The domain thus spans a range of variability in canopy structure and topographic conditions over a rather small area, which is common in the sub-alpine environment.

The site is at ~5 km distance to well-established and predominantly flat research sites that have hosted recent experimental forest snow process studies from the WSL Institute for Snow and Avalanche Research (SLF), including Laret (Malle et al., 2019; Webster, 2016), Seehornwald (Webster et al., 2016), and Ischlag (Moeser et al., 2015). The sites from Koutantou et al. (2022) are fully contained in the perimeter of this study. ~~The~~ ~~O~~operational measurements from the automatic weather station (AWS) Davos (DAV) and from the measurement field at Weissfluhjoch (WFJ) are within 1 km and 3 km of the site, respectively (Figure 1a).

2.2 Modelling framework

Snow cover simulations with the Flexible Snow Model FSM2 (Mazzotti et al., 2020b, a) are at the core of this study's methodology (Figure 2). FSM2 is the upgrade of the physics-based, medium-complexity Factorial Snow Model, FSM (Essery, 2015), with forest canopy added. It includes all major canopy processes (interception of snow in the canopy, subsequent unloading and sublimation, shortwave radiation transfer, longwave radiation enhancement, and wind attenuation) with well-established parametrizations. We applied~~y~~ the version presented by Mazzotti et al. (2020a) specifically developed for hyper-resolution (meter-scale) simulations, FSM2.0.3. This version uses process-specific canopy metrics, computed for each modelled location. Notably, insolation through the three-dimensional forest canopy is explicitly represented by importing time series of transmissivity for direct shortwave radiation from an external radiative transfer model. This allows achieving the accuracy of very detailed, ray-tracing-type radiative transfer modelling approaches without compromising the complexity and computational efficiency of FSM2. For this study, we ~~run~~ ran FSM2 at 2 m grid spacing (i.e., 850'000 points) and hourly resolution for six winters (i.e., water years (WY) 2016-2021). Our model application follows Mazzotti et al. (2021), who used equivalent hyper-resolution simulations to explore model upscaling behavior.

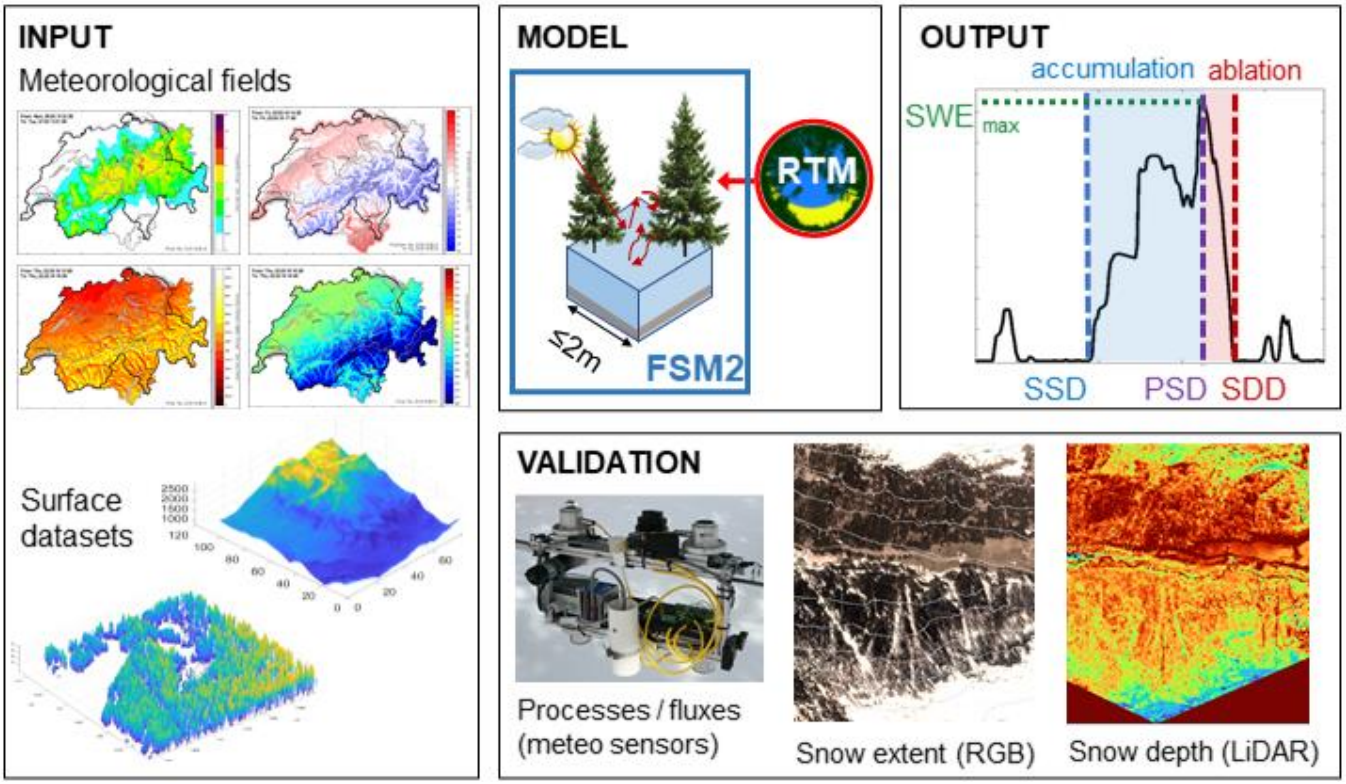

Figure 2: Conceptual sketch of the study methodology. Input meteorological and surface datasets (from the OSHD and the 2017 LiDAR mission, Section 2.2), FSM2 including external radiative transfer model, evaluation approaches (presented in Mazzotti et al. 2020a and Section 2.3) and resulting snow cover dynamics descriptors: peak SWE (SWEmax), start of snow cover period (SSD), day of peak SWE (PSD) snow disappearance date (SDD) - see Section 2.4 for definitions.

LiDAR datasets acquired through airborne laser scanning (ALS) in 2017 in the context of the first European mission of the Airborne Snow Observatory (ASO, Painter et al., 2016; Mazzotti et al., 2019a) provided the basis for computing all canopy metrics required by FSM2.0.3, including vertically projected canopy cover, canopy height, canopy density (i.e. LAI), and sky-view fraction in the full hemispherical view, for details see Mazzotti et al. (2021, 2020b) and Supplementary Material S2. Shortwave transmissivity time series at each location were obtained with the workflow from Webster et al. (2020), which calculates transmissivity through an overlay of a hemispherical image and solar position at any given point in time, as presented by Jonas et al. (2020). In Webster et al. (2020), LiDAR-derived synthetic hemispherical images based on a methodology originally proposed by Moeser et al. (2014) wea~~a~~re used for this purpose. Through point cloud enhancing techniques, the resulting images capture the shape and fine-scale structure of every individual tree in the surrounding, enabling highly accurate calculations of subcanopy radiation (Figure S3.2). The workflow was calibrated using real hemispherical images at our sites and using the same LiDAR data (Koutantou et al., 2022), allowing direct application also in this study. Additional surface datasets (e.g., elevation) were available through SLF's Operational Snow-Hydrological Service's (OSHD) modelling framework. These data were provided at 25 m resolution and interpolated to the model resolution (2 m).

Meteorological forcing was also available through OSHD. As described by Griessinger et al. (2019), gridded data of all necessary meteorological input variables (incoming short- and longwave radiation, air temperature and relative humidity, wind speed, rain- and snowfall rates, and atmospheric pressure) wea~~a~~re provided by MeteoSwiss (COSMO-1 product) at hourly interval and 1-km resolution over all of Switzerland and further downscaled to model resolution. Additional corrections (for biases or terrain effects) wea~~a~~re applied to some of the variables, e.g., wind speed (Winstral et al., 2017) and shortwave radiation (Jonas et al., 2020). We refer to Griessinger et al. (2019) for details. By leveraging OSHD methods, this study benefitted from the currently best meteorological forcing datasets available for the site, exploiting latest downscaling approaches specifically developed for snow modelling in complex terrain. Here, input fields were initially downscaled to 25 m and subsequently linearly interpolated to 2 m resolution.

2.3 Valid~~erific~~ation of model use case

FSM2's capability to accurately simulate sub-canopy snow energetics and to thus reproduce realistic small-scale forest snow cover dynamics has been demonstrated in a dedicated study (Mazzotti et al., 2020a). Their detailed model validation was done in the vicinity of our study area, with the same type of input data, and for the same type of canopy data. A summary of the validation approach and results is provided in the Supplementary Material S3. For this reason, another model validation is beyond the scope of this study; nevertheless, an assessment of our simulations against available snow distribution datasets was performed to ensure plausibility of the model application for our use case. We ~~use~~ considered four independent data sources: (1) Daily now depth data from stake readings acquired next to automatic weather stations (AWS) in Davos and Weissfluhjoch to assess the simulations at open sites; (2) High- and medium-resolution satellite RGB imagery available through Planet Explorer (www.planet.com) at approx. weekly intervals for the last five modelled WY's, including Landsat 8, Sentinel-2 and PlanetScope, to evaluate modelled snow cover extent during periods of partial snow cover; (3) Maps of sub-canopy snow depth over the full domain from two of the 2017 ASO LiDAR acquisitions (see Section 2.2) at 3 m spatial resolution, parts of which were used by Mazzotti et al. (2019a); and (4) Time series of sub-canopy snow depth maps over two 150 x 150 m domains (see Figure 1) on the two opposed slopes obtained with UAV-borne LiDAR in 2020, presented by Koutantou et al. (2022). For details on the LiDAR campaigns, the reader is referred to the corresponding publications.

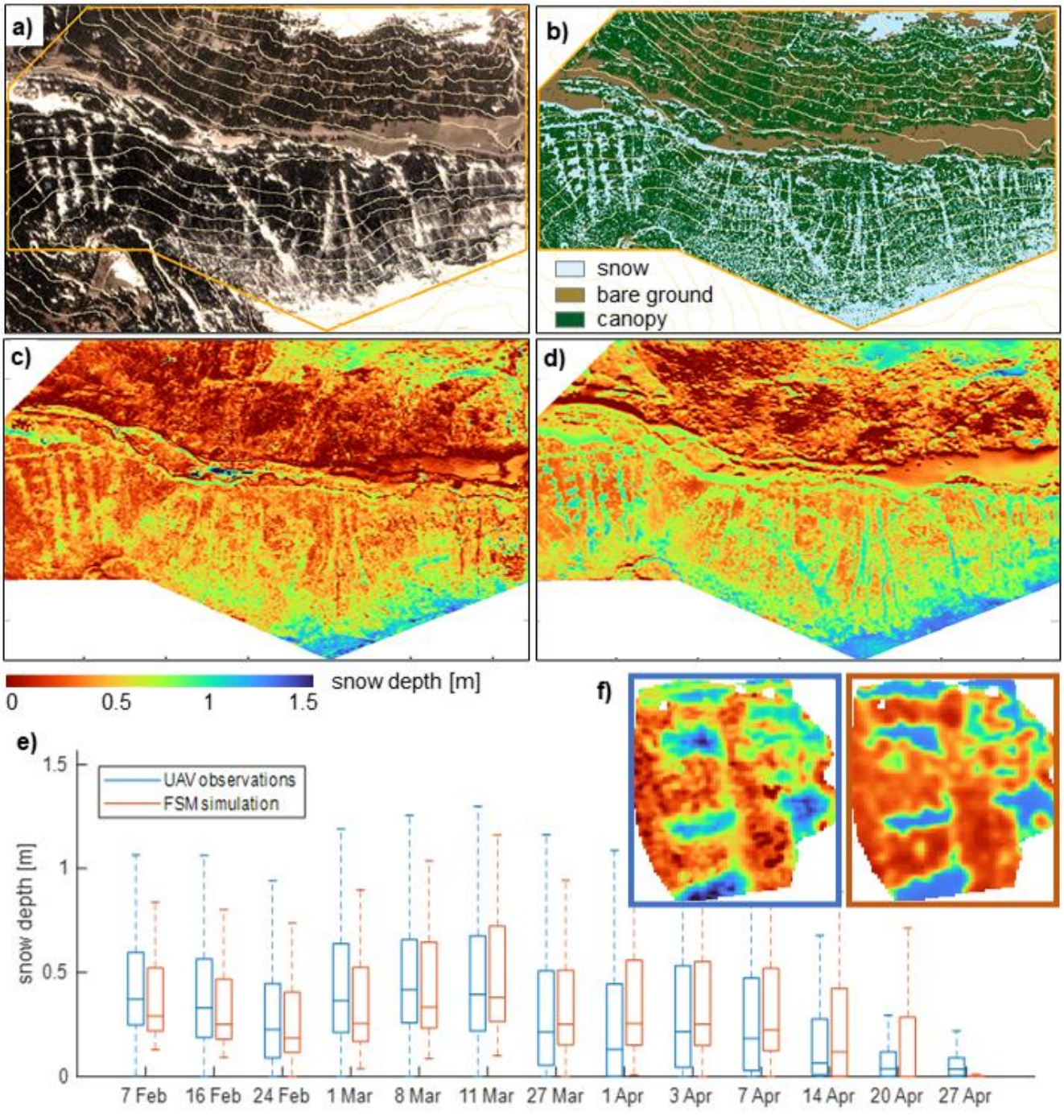

Figure 3: Examples of plausibility checks performed to verify the model use case, including comparisons of 1) satellite RGB imagery acquired by Planetscope on 28. April 2018 (a) and snow cover extent simulated by FSM2 on the same day (b); 2) snow depth distribution derived from ALS data (c) and simulated by FSM2 (d); and 3) snow depth statistics of UAV-LiDAR derived snow maps at the north-exposed site and resulting from FSM2 (e) and observed and modelled spatial distribution of the 8 March 2020 campaign (f).

Figure 3 presents examples of visual comparisons of model simulations to satellite (Figure 3a-b), ALS (Figure 3c-d) and UAV-LiDAR data (Figure 3e-f). These assessments reveal that the model captures the general characteristics of snow depth and snow disappearance patterns well. The strong temporal lag in snow disappearance between the south- and the north-facing slope is clearly visible in the satellite imagery and likewise reproduced by the FSM2 simulations. Snow distribution features such as preferential ablation along south-exposed forest edges and higher snow amounts in canopy gaps compared to nearby under-canopy locations in the north-exposed slope are also clearly present in both the LiDAR datasets and the simulations. Overall, the ~~verification confirms~~validation supports that FSM2 simulations are suitable for this use case. Goodness of fit measures would be confounded by uncertainties in meteorological input and snow measurement inaccuracies (see e.g. Raleigh et al., 2015; Günther et al., 2019; Currier et al., 2019) and were therefore not considered here.

2.4 Analysis approach

Our analysis uses several descriptors of the snow season and of the surface energy exchange processes derived from the FSM2 simulation results. These metrics we~~a~~re computed at each modelled location (i.e. 2 m grid cell) for all winters as follows.

1. *Peak SWE:* The maximum value of snow water equivalent on the ground attained over the course of a snow season / WY.
2. *Day of peak SWE (PSD):* The day on which peak SWE occurred. In case of multiple occurrences of peak SWE over the season, the median was selected.
3. *Accumulation period:* Period between the last occurrence of SWE < 10 mm prior to peak SWE and the day of peak SWE.
4. *Start of snow cover period (SSD):* The first day of the accumulation period.
5. *Ablation period:* Period between the day of peak SWE and the first occurrence of SWE < 10 mm following peak SWE.
6. *Snow disappearance day (SDD):* The last day of the ablation period; also referred to as melt-out.
7. *Snow cover duration:* The number of days between the start of snow cover and snow disappearance.
8. *Ablation rate:* The quotient between peak SWE and the length of the ablation period.
9. *Cumulative ablation:* Amount of SWE depleted over the course of a specific time interval (computed as sum of SWE decrements including losses due to both melt and sublimation).
10. *Average surface energy fluxes:* Incoming and net short- and longwave radiation as well as turbulent (sensible and latent) heat fluxes into the snowpack, averaged over a specific time interval, where positive fluxes indicate transport towards the snow surface.

Note that the temporal integration varies for different metrics, with some applying to the point-specific snow cover durations and some integrating over fixed time intervals. The choice of temporal integration interval wa~~i~~s motivated by the purpose of the corresponding analysis. Moreover, it should be noted that the definition of contiguous accumulation and ablation periods until / from peak SWE, as applied here, implies that melt events can occur during the accumulation and snowfall events during

the ablation periods, respectively. The 10mm threshold applied to define snow vs. no-snow conditions served to ensure that only days with snow present throughout the whole day would be included in the analysis of ablation rate and surface energy fluxes.

To assess relationships of any snow or process descriptor to canopy structure, we quantified~~y~~ the fine-scale canopy structure at a point in terms of local canopy cover fraction, one of the canopy metrics provided as input to FSM2 ('fveg', see Mazzotti et al. (2020b)). This variable describes the fraction of the vertically projected canopy cover within a 5 m radius around each modelled location, taking values between 0 and 1. We used local canopy cover fraction because it was shown to be strongly correlated to small-scale snow depth distribution at flat sites (Mazzotti et al., 2020b) and in steep terrain (Koutantou et al., 2022).

3 Results

The following sections present a systematic analysis of FSM2 simulation results, aimed at illustrating the interplay of canopy structure, topographic, and meteorological controls. We first provide a general overview of snow cover dynamics across the site for all simulated years to provide context (Section 3.1), then consider the spatial distribution of our snow descriptors in more detail (Section 3.2). To help interpret spatial patterns, we analyse the combined impact of the physiographic factors, topography and canopy structure, first on the temporal evolution (Section 3.3) and then on the spatial distribution (Section 3.4) of snow cover dynamics and the underlying processes. Finally, we explore the impact of meteorological conditions on the temporal consistency of said spatial patterns between water years (Section 3.5).

3.1 Overview of simulated snow cover dynamics

Figure 4 summarizes the statistics of the different snow season descriptors for all simulated years, aiming to give an overview of their within-year variability (attributable to variations in canopy structure and topography), and of their between-year variability (attributable to variations in driving meteorology). A summary of meteorological conditions during the simulation period is provided in the Supplementary Material (Figures S3.1-3.2). The start of continuous snow cover strongly varies both across the model domain and between the years (Figure 4a). The medians within the model domain vary by 2 months, ranging from 5 November (WY 2019) to 5 January (WY 2017). Noteworthily, the spread of the start of snow cover varies strongly between the simulated WYs as well. While in three years snow cover onset happens basically simultaneously across the entire domain (WYs 2017, 2018, 2019), partial melt-out during snow accumulation cause heterogeneous snow cover onset dates across the domain in the other years, with interquartile ranges of full snow cover onset of over a month.

The timing of peak SWE (Figure 4b) is, on average, much more consistent over the years, with median peak SWE ranging from 11 March (WY 2020) to 1 April (WY 2018). However, the spread across the model domain in each year can be large (interquartile range of approx. 2 months in WYs 2019 and 2021), which means that there can be a considerable temporal offset in the start of the ablation period across the site. Notably, this leads to some locations reaching peak SWE only when others

have melted out already (overlap of boxes for day of peak SWE and snow disappearance day of the same year). The rather large spread in snow disappearance day within each year (Figure 4c), with interquartile ranges between 2 and 6 weeks, is the result of spatial variability in both accumulation and ablation rates and is thus not surprising. Between-year variability in melt-out timing is much larger than for timing of peak SWE, with medians between 10 April (WY 2016) and 26 May (WY 2019). Further, also peak SWE itself varies (Figure 4e), with median peak SWE across the model domain between 135 mm (WY 2016) and 314 mm (WY 2019), mostly reflecting years with higher and lower snowfall, respectively. Notably, interquartile ranges are not systematically higher or lower for higher or lower median peak SWEs occurrences.

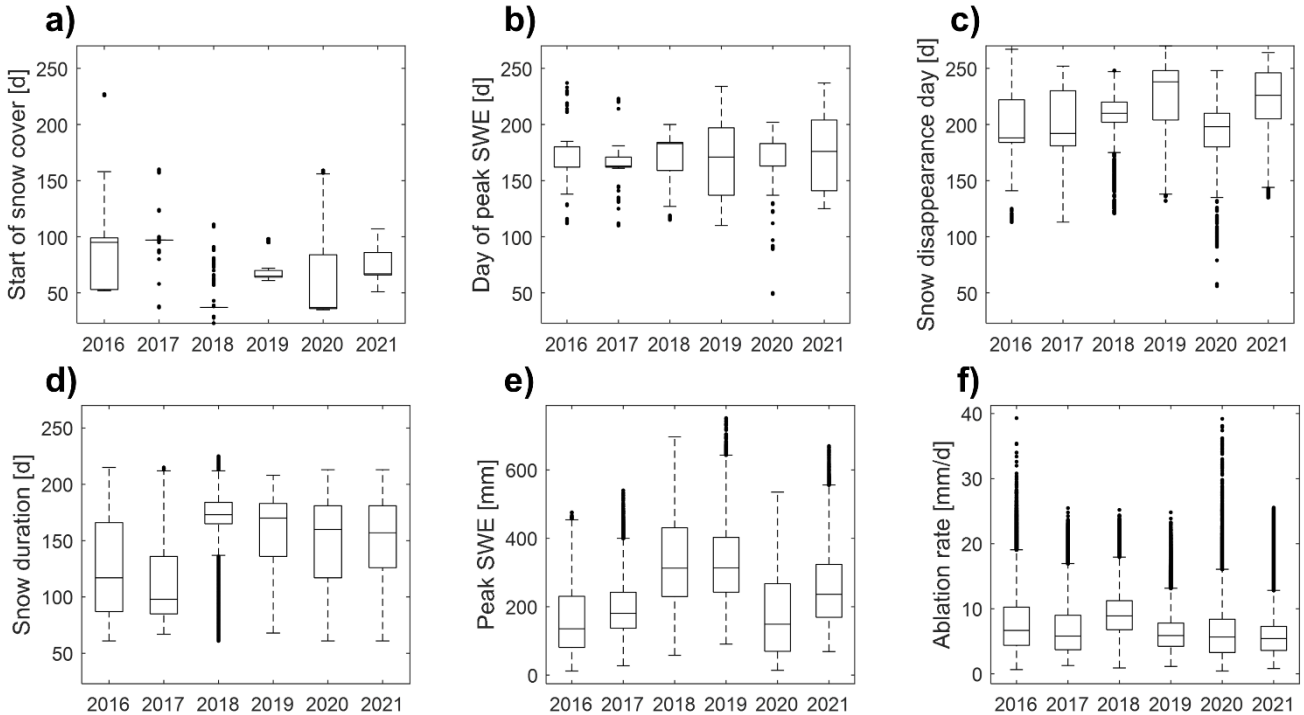

Figure 4: Summary statistics of snow season descriptors across the full model domain and for all simulated water years (WY), including (a) the start of snow cover period, (b) day of peak SWE, (c) snow disappearance day, (d) duration of full snow cover, (e) peak SWE, and (f) ablation rate. Descriptors denoting specific points in time (a-c) are indicated in terms of day since October 1st.

The combination of the variable start of snow cover and snow disappearance days implies highly variable snow cover durations (Figure 4d). Median full snow cover duration across the model domain varies between 96 (WY 2017) and 173 (2018) days, and interquartile range varies between 19 (WY 2018) and 65 (WY 2020) days. Snow cover duration can also be interpreted as the combination of amount of SWE to be depleted and efficiency of ablation processes. Notably, ablation rates (Figure 4f) are more uniform across the WYs (median 5.5-9 mm/day) but still rather variable across the model domain (interquartile ranges of 3.6-5.9 mm/d).

It should be highlighted that there does not appear to be any clear link between any of the individual snow cover descriptors; for instance, higher peak SWE does not seem to imply longer snow duration, and later snow disappearance is not linked to

higher ablation rates. Essentially, this is a consequence of accumulation and ablation processes being affected by different meteorological drivers.

3.2 Spatial patterns of snow cover dynamics

The l~~L~~arge spread in the boxplots in many of the subpanels of Figure 4 indicates that most snow season descriptors exhibit strong spatial variability across the model domain during most years. In Figure 5, we present spatial maps of the same snow season descriptors for WY2019 to analyse the full spatial patterns behind this variability. To better demonstrate the spatial details, we zoom in to a sub-domain (Figure 1) that comprises the entire range of canopy covers, elevation ranges, slopes, and aspects, yet representing the physiographic character of the entire domain well. Equivalent plots over the full model domain are included in the Supplementary Material (Figures S5.1-5.3) for interested readers.

Figure 5 illustrates how peak SWE, ablation rates, day of peak SWE, and snow disappearance date vary across the landscape as a function of canopy and within the complex topography. The link between peak SWE and canopy structure (Figure 5a vs 5b) is obvious and reflects the impact of snow interception by the canopy on accumulation, which scales with local canopy cover. This dependency is well visible when comparing peak SWE at under-canopy vs. open / gap locations (Figure 5b). Yet, a closer look at the gaps and forest edge areas (especially in the upper, south-exposed part of the domain) reveals a rather large spread in peak SWE for these locations with low to no local canopy cover, even within this relatively small subdomain of 1.5 km^2. For this specific example, the spread in peak SWE amounts to approx. 200 mm. Consequently, canopy structure is clearly not the only factor controlling peak SWE distribution, despite the strong correlation between peak SWE and local canopy cover fraction with Pearson's correlation coefficient (R) ranging from -0.89 (2018) to -0.76 (2017). Note that correlation coefficients are computed over the full model domain.

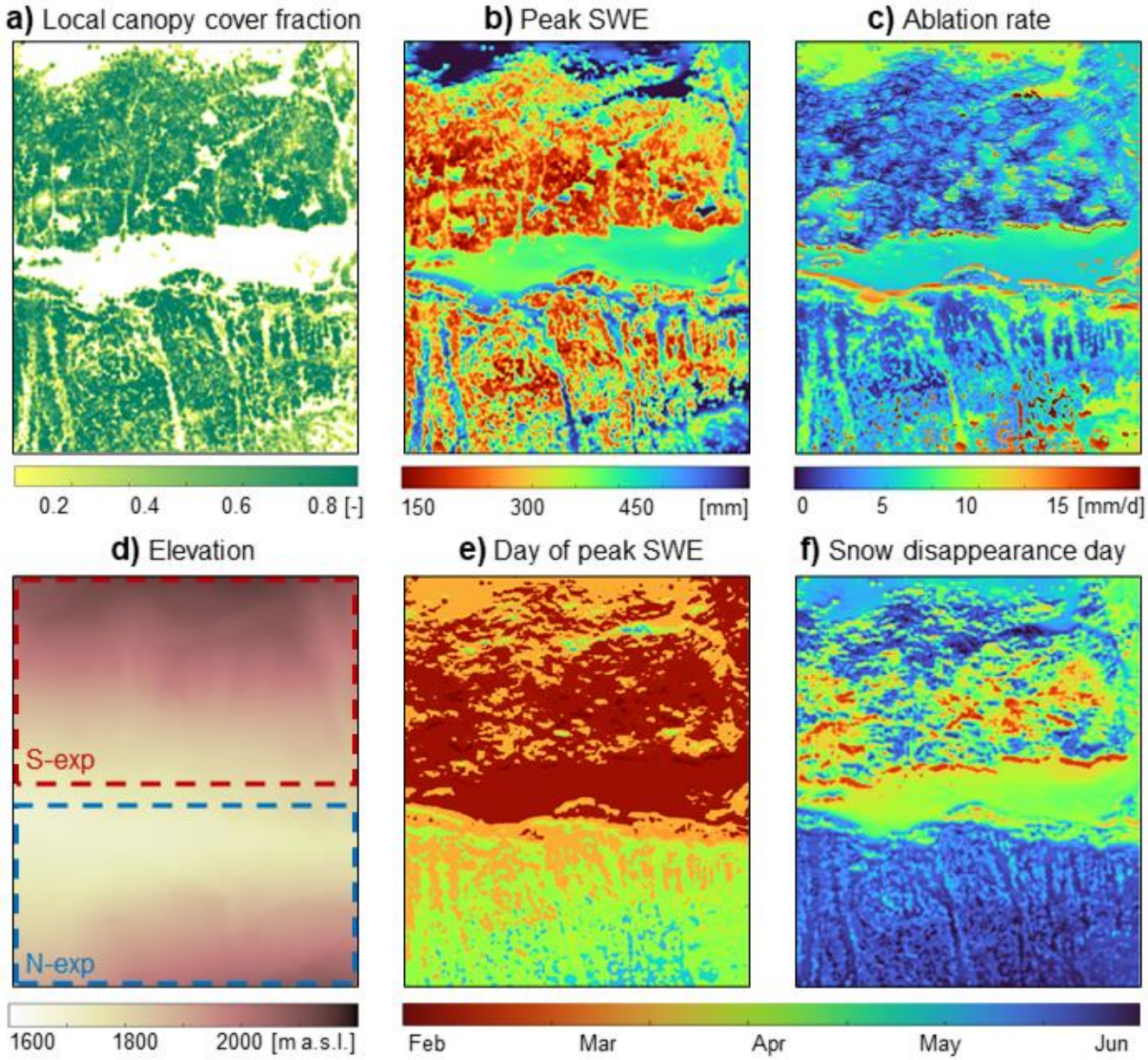

Figure 5: Canopy cover (a) and topographic (d) maps, as well as snow season descriptors including peak SWE (b), ablation rate (c), day of peak SWE (e) and snow disappearance day (f), for a sub-section of the model domain and WY 2019.

When interpreting spatial patterns of peak SWE, it is important to consider that the timing of peak SWE also varies across the domain (i.e., ablation starts in some areas while others are still accumulating snow; Figure 5e). Generally, the onset of the ablation period occurs earlier on the south-exposed slope. The earliest onsets occur along the canopy edge at lower elevations, but there is no evident simple relationship with canopy cover. The combination of strong variability in peak SWE and

heterogeneous peak SWE timing means that spatial patterns of ablation rates (Figure 5c) and snow disappearance date (Figure 5f) are complex, with non-trivial dependencies with either canopy cover or topography (Figure 5d).

Notably, snow disappearance day is more variable on the south-exposed slope than in the north-exposed slope, where snow disappearance is restricted to a shorter time span. Complex melt-out patterns on the south-exposed slope hint at considerable spatial heterogeneity in ablation processes which override accumulation patterns, so that the spatial structure of snow disappearance is considerably different from that of peak SWE (Figure 5b vs 5f, upper part). In contrast, this is not the case on the north-exposed slope: Here, under-canopy areas melt out earlier than canopy gaps, which means that melt-out patterns generally have a similar spatial distribution as accumulation patterns (Figure 5b vs 5f, lower part). These similarities suggest that on the north-exposed slope spatial variations in ablation rates are not strong enough to supersede spatial variations in accumulation. We will look at the physical processes that drive these patterns in more detail in the following sections.

Ablation rates (Figure 5c) exhibit spatial patterns that do not correspond to any other snow season descriptor. Remarkable features are the maxima along the south-facing canopy edge on the south-exposed slope, and in the canopy gaps on the higher-elevation areas of the north-exposed slope. This is where snow generally either starts to melt first or last (compare to Figure 5e). Furthermore, large canopy gaps on both slopes generally feature higher ablation rates than adjacent under-canopy areas. Note that assessing the dependencies of ablation rate on canopy structure and topography is confounded by the necessity to calculate ablation rates over the local ablation period (see definition in Section 2.4), which itself varies across the domain due to variable timings of peak SWE and snow disappearance.

3.3 Impact of canopy structure and topography on the temporal evolution of the snow cover and underlying processes

The analysis in Section 3.2 clearly suggests that the interaction between canopy structure and topography plays a relevant role in shaping spatial snow cover dynamics. To understand these patterns and the processes that lead to them, it is instructive to consider time series of snow cover evolution at some representative locations. We manually selected seven locations that cover the existent range of canopy structures and topographic settings to showcase potential outcomes of process interactions in a systematic way. We include points located at the north- and south-facing edges of canopy gaps for both north- and south-exposed slopes, as well as three points located under canopy (two on the south- and one on the north-exposed slope; the two points on the south-exposed slope differ in their proximity to a sun-exposed canopy edge, where point 1 is more sun-exposed and point 2 more shaded). The locations of these points are marked in the Supplementary Material (Figure S6). Figure 6a shows SWE at these seven locations for WY 2019. Note that we will look at data from other years and the influence of weather on inter-annual differences in Section 3.5.

At the beginning of the accumulation period, all three points that are located under canopy accumulate less snow than all points located in gaps. These two distinct pathways reflect the fact that, if no major precipitation gradients exist across the site and if ablation processes or the impact of wind redistribution is negligible, interception of snow is the only process that introduces spatial variability during this phase. Canopy structure thus exerts the primary control on snow accumulation. However, as the season progresses, further pathways fork off. In this example, early onset of ablation at two points on the south-exposed slope

results in further spatial segregation. The first point (dark red), which reaches peak SWE by mid-February, is located under canopy close to a south-facing canopy edge. The second point (light green), which reaches peak SWE in mid-March, is located at the south-facing edge of a forest gap. These findings showcase that the same canopy structure configuration can host different snow evolution pathways in different topographic settings. This creates more variability in snow cover evolution pathways on the south-exposed slope (here, points at south- and north-facing canopy edges diverge), and limited variability on the north-exposed slope (here, points at south- and north-facing canopy edges do not diverge).

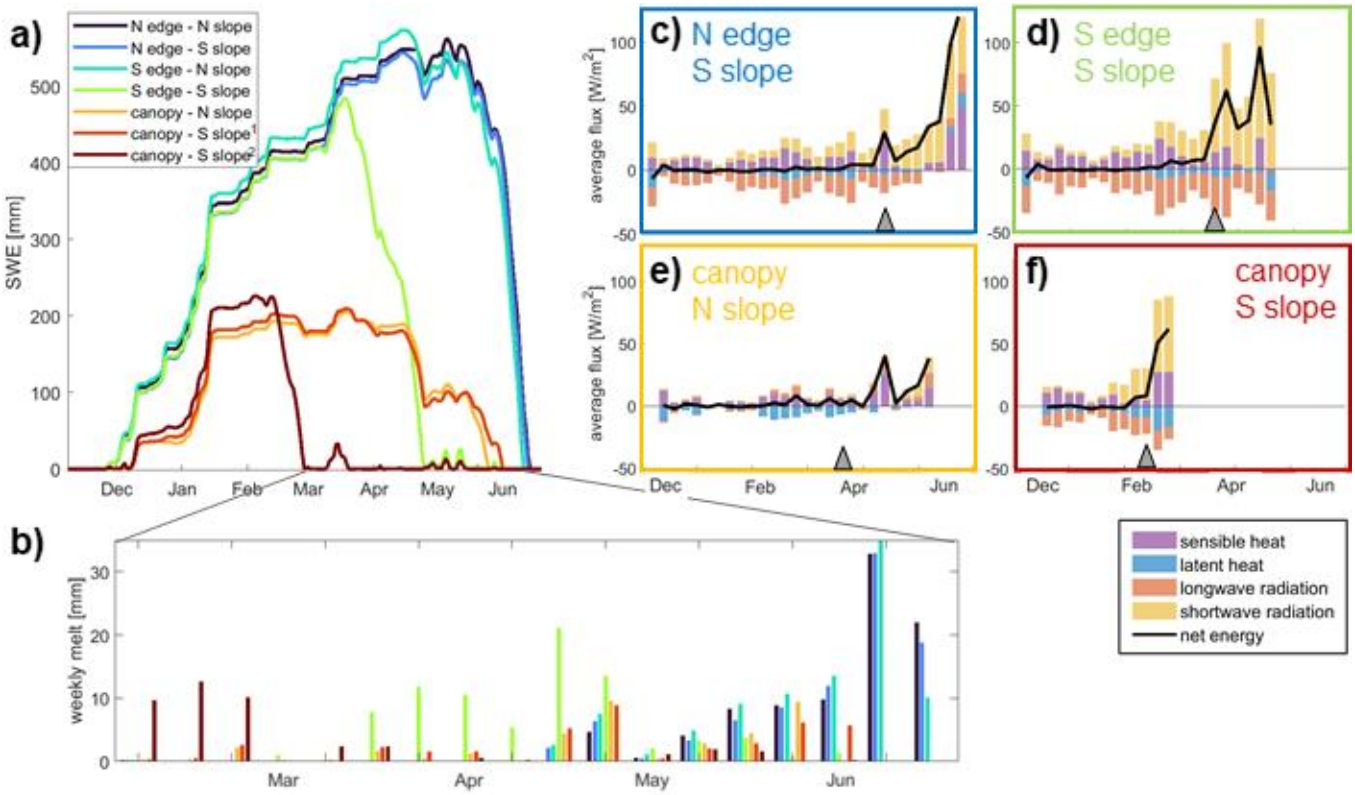

Figure 6: Interactions between canopy structure and topography illustrated at seven example points (locations see S3). Time series of SWE (a), weekly melt during the ablation period (b) and surface energy balance partitioning at four of the points (c-f). In c-f, bars show weekly average fluxes, while the black line depicts their sum, grey triangles mark the day of peak SWE, and only periods with snow on the ground are shown.

While accumulation patterns are mainly dictated by canopy structure, topography comes into play when ablation processes start. Melt requires a positive net energy input to the snowpack, which is the result of multiple superimposed fluxes. To elucidate the underlying processes, Figure 6c-f show surface energy balance partitioning over time at four of the seven points, which cover the four major snow cover evolution pathways seen in Figure 6a. These plots show that at all points prior to the onset of the ablation period, net shortwave radiation and sensible heat generally provide positive contributions, while latent heat provides a negative contribution. Net l~~L~~ongwave radiation acts as a compensating flux. It is strongly negative at locations in canopy gaps (large sky-view, i.e., little longwave enhancement, Figure 6c+d) as well as under-canopy locations that receive

positive net shortwave radiation and sensible heat contributions. In contrast, ~~it~~ net longwave radiation is positive where other positive fluxes only constitute negligible contributions (i.e., under-canopy, shaded locations, Figure 6e). At both points where ablation starts early, regardless of canopy structure, its onset is due to an increase in net shortwave radiation that can no longer be compensated by a negative net longwave radiation flux. Exposure to shortwave irradiance early in the snow cover period is thus a mechanism by which topography can affect snow cover evolution pathways in addition to canopy structure, either by way of terrain shading or due to inclined terrain (towards or away from sun). At points where direct insolation is unavailable early in the snow cover period and ablation starts later, the driving mechanisms are different. At under-canopy points, positive net longwave radiation contributions and sensible heat drive melt; at gap locations, net shortwave radiation and sensible heat constitute the strongest positive fluxes.

Generally, shortwave radiation driven ablation leads to larger net energy turnover and therefore high ablation rates even early in the season (Figure 6b). This can create situations where snow in canopy gaps can melt out earlier than snow under canopy, despite peak SWE being higher (Figure 6a, light green vs light red). Early-season insolation is hence the driver by which spatial heterogeneity in ablation processes can override accumulation patterns on the south-exposed slopes (c.f. Section 3.2). Not surprisingly though, the highest ablation rates are in the late season in gaps when all fluxes are positive. Yet these high ablation rates do not impact melt-out patterns, because by this time gaps on the north-exposed slopes are the only areas with snow left.

3.4 Impact of canopy structure and topography on the spatial distribution of leading processes

The snow cover evolution pathways and corresponding energy balance partitioning pathways shown in Section 3.3 illustrate the interaction between canopy structure and topography. Considering how these pathways are distributed in space puts the snow cover descriptor maps from Figure 5 in context. An important insight from Section 3.3 is that exposure to early-season shortwave radiation majorly affects snow cover dynamics, which leads to contrasts between opposing slopes that are or are not affected by terrain shading. Figure 7 shows maps of canopy cover, average shortwave irradiance, all-wave irradiance, and cumulative snow ablation between mid-January and end of February for WY 2019 across the two opposing slopes. This period was chosen because it falls between the start of the snow cover period and median day of peak SWE, which makes it suitable for analysing the occurrence and distribution of early-season ablation.

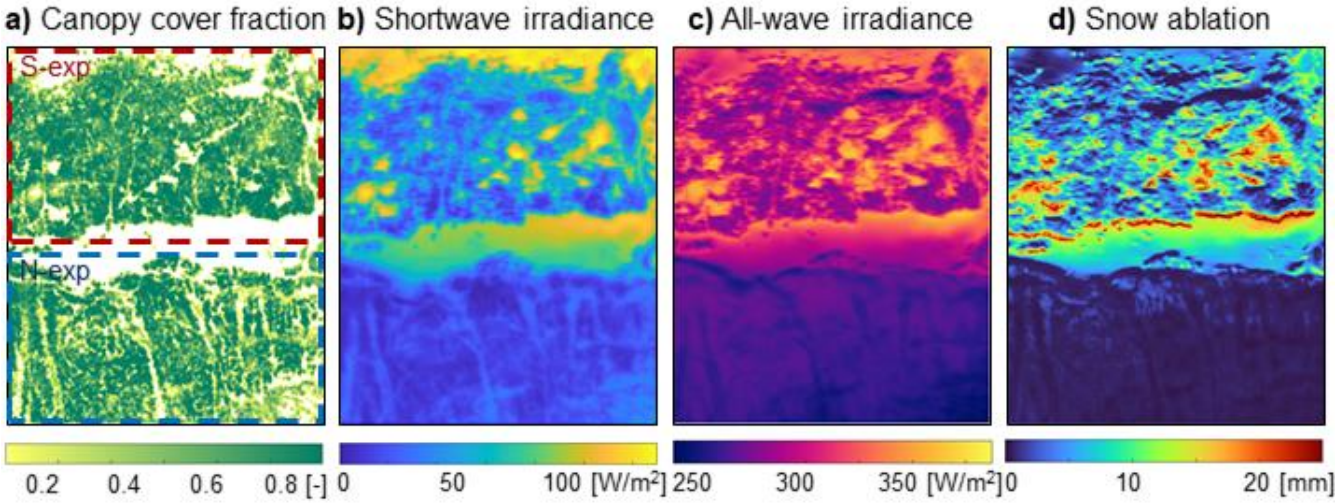

Figure 7: Canopy cover fraction and aspect in the sub-domain (a), average incoming shortwave (b) average all-wave irradiance (c), and cumulative SWE ablation (d) between mid-January and end of February for WY 2019.

In early winter, shortwave irradiance controls all-wave irradiance patterns (Figure 7b vs. 7c; see also Figure S5.2 in Supplementary Material), and ablation largely matches these patterns (Figure 7d), confirming that early-season shortwave irradiance is a prerequisite for early-season ablation. Due to topographic shading, only the south-exposed slope receives direct shortwave irradiance at this time of the year. Consequently, topography exerts a primary control on early-season ablation. On top of that, canopy shading affects the distribution of shortwave irradiance, but during times with low solar elevation angles the dependency between canopy structure and direct shortwave radiation is complex. In fact, early in the season the correlation between shortwave irradiance and local canopy cover is rather low (R = -0.52). This, in turn, entails local canopy cover and snow ablation to be uncorrelated as well (R = 0.05). These low correlations imply that early-season ablation may potentially counteract and even disrupt the association of peak SWE patterns and local canopy cover identified in Section 3.2 (see Figure 5).

Shortwave irradiance is, however, not the only flux determining ablation patterns. Figure 7 reveals that some areas above the tree line on the south-exposed slope do not experience early-season ablation, despite the high shortwave radiation input. This indicates that net energy input must be reduced by other negative fluxes. Additionally, the energy balance partitioning plots in Figure 6 evidence other positive contributions to net energy input to the snowpack. To visualize the spatial structure of these contributions, Figure 8 shows each individual surface energy balance component (net short- and longwave radiation, sensible and latent heat fluxes) for periods early (Figure 8a) and late (Figure 8b) in the season (WY 2019), as well as the corresponding net surface energy flux (Figure 8c). The spatial distribution of individual energy fluxes and their evolution in time generally conform with findings from Figure 6, with sensible heat as the only other positive contribution early in the season and longwave transitioning into a positive flux especially at under-canopy locations and later in the season. Overall, Figure 8 demonstrates how spatial patterns of individual fluxes translate to patterns of net surface energy, which largely match shortwave radiation

patterns in both periods. Figure 8d displays correlation coefficients between net surface energy and individual energy balance components as they evolve over the season. The strongest positive correlations to shortwave radiation are confirmed, while correlations to longwave radiation are consistently and increasingly negative. No systematic link between net energy and turbulent fluxes is evident.

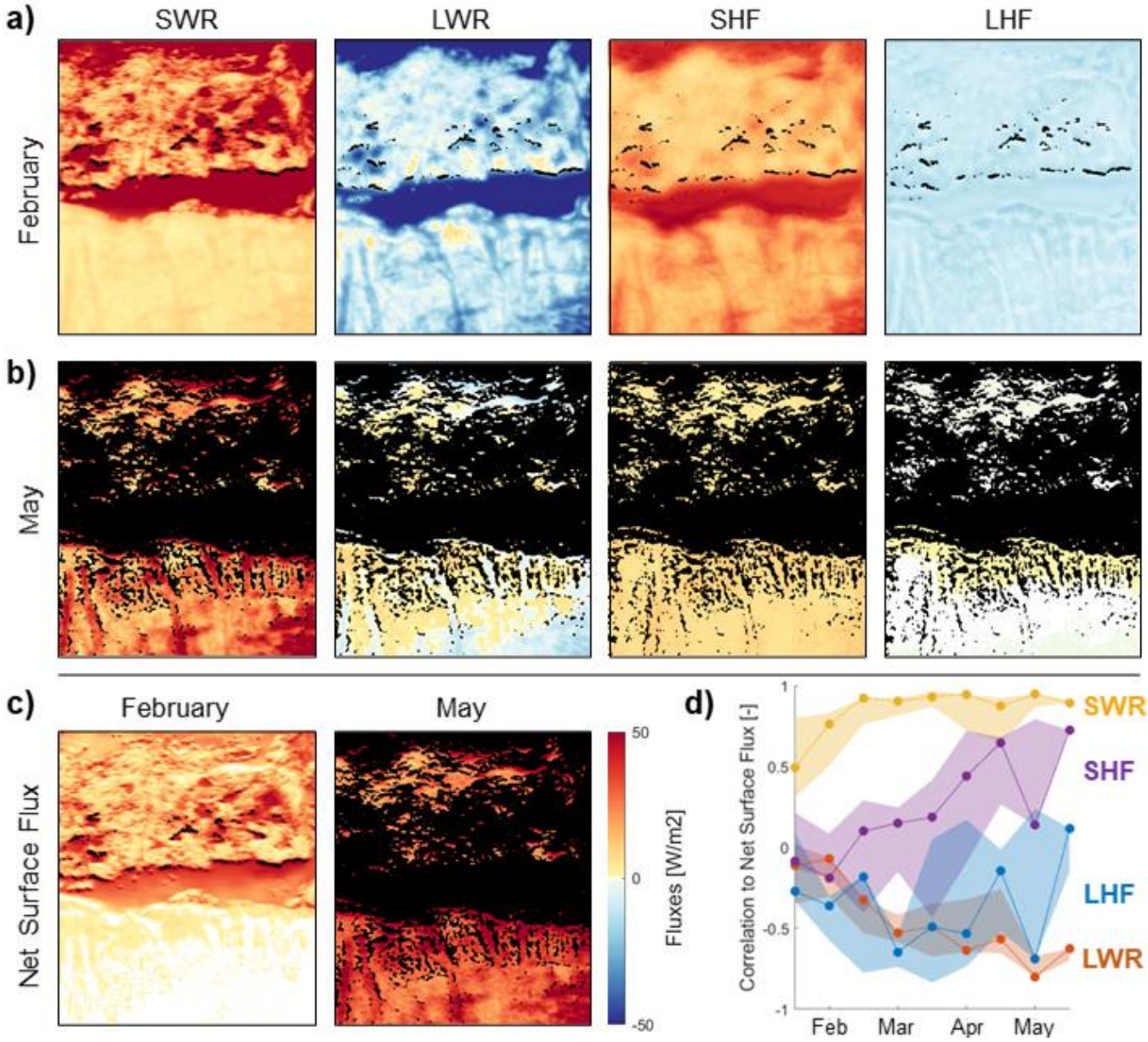

Figure 8: Energy flux partitioning into the four surface energy balance components (net short- and longwave radiations, SWR and LWR; sensible and latent heat fluxes, SHF and LHF) for two weeks in February (a) and May (b) 2019, respectively, as well as net energy flux at the snow surface (c), areas that have melted out by the time shown are marked black; Correlations (Pearson's R) between individual energy fluxes and net surface energy over the season (d), with lines showing WY 2019 and shaded areas the range of all modelled WYs.

3.5 Impact of meteorological conditions on the temporal consistency of spatial patterns

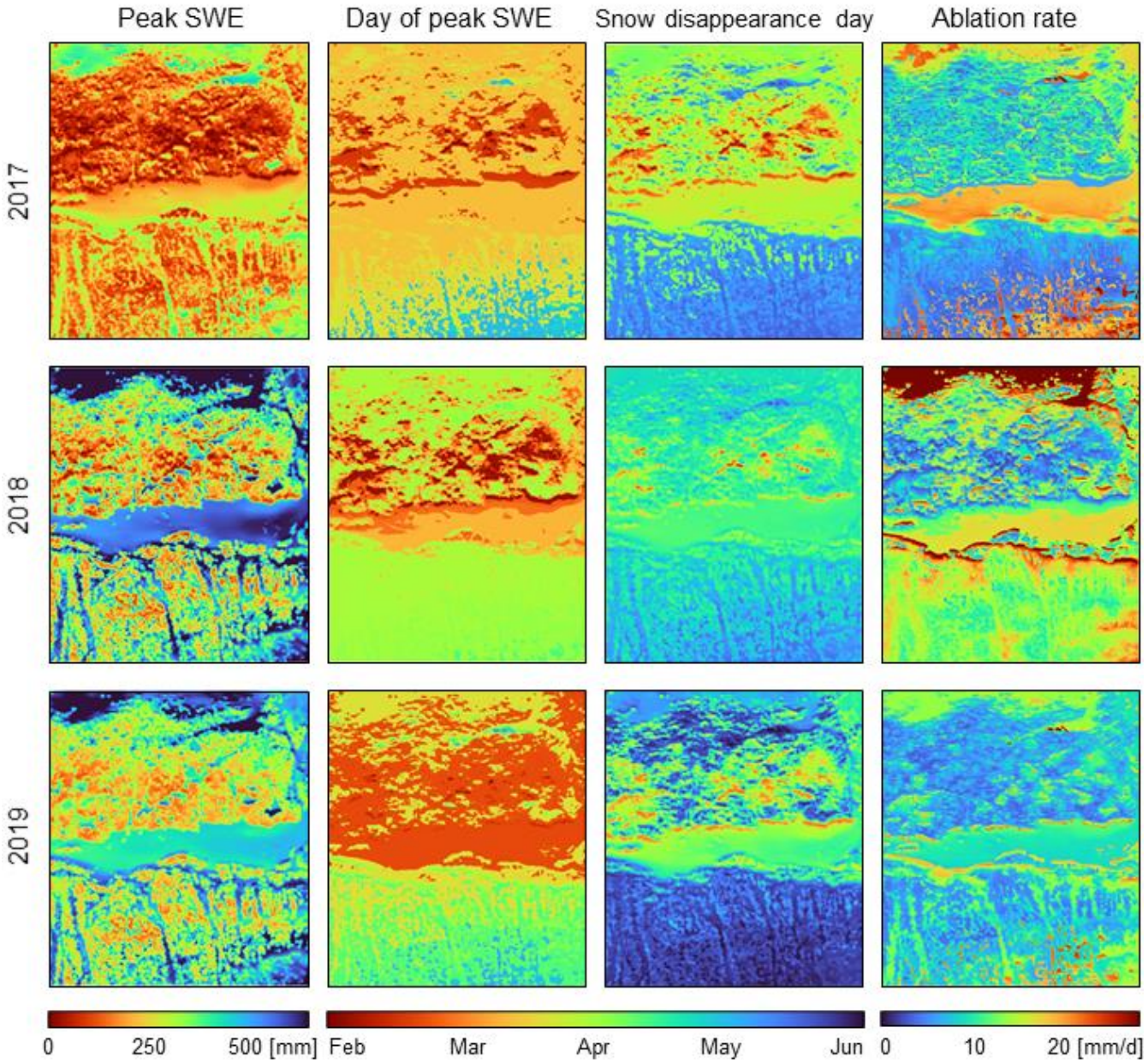

Figure 9: Spatial patterns of snow season descriptors for the sub-domain, including peak SWE (1st column), day of peak SWE (2nd col.), snow disappearance day (3rd col.) and ablation rate (4th col.) during three different WYs, namely 2017 (1st row), 2018 (2nd row) and 2019 (3rd row).

Meteorological conditions and their variability between years alter the relative magnitude and timing of different processes. By doing so, they can potentially impact the consistency of snow cover dynamics and resulting spatial patterns. Figure 9 shows

the spatial distribution of the same snow cover descriptors shown in Figure 5, but now including three different WYs. Full domain maps of all WYs are available in the Supplementary Material (Figures S7.1-S7.5). For all snow season descriptors, we find both temporally consistent and inconsistent features. The link between canopy structure and peak SWE is evident in all years, despite stronger imprints of early-season ablation patterns in some years (e.g. 2018 vs. 2019). In fact, the autocorrelation between peak SWE patterns of different years is high (R: 0.94-0.98). In contrast, ablation rate patterns are generally uncorrelated (R: 0.07-0.79). Ablation rate maxima are found at different locations of the domain in different years. For example, maximum ablation rates in WY 2018 were above the tree line on the south-exposed slopes but were in canopy gaps on the north-exposed slope in both WYs 2017 and 2019. Below-canopy areas have comparatively low ablation rates in all years, but differences between slopes are more pronounced in WY 2018 than in 2017 and 2019. These consistencies and inconsistencies are likely affected by differences in the timing of the ablation period.

In terms of the timing of peak SWE and snow disappearance, the temporal sequence in which different locations melt out is mostly consistent between years: South-exposed canopy edges and under-canopy locations generally become snow-free first, and snow lasts longest in shaded canopy gaps (i.e. those on north-exposed slopes). However, the timing of and days between both peak SWE and snow disappearance across the domain vary. For example, distribution of peak SWE day in 2019 is, in the first order, bimodal, with a clear separation between the south- and north-exposed slopes; also in 2017, the distribution of peak SWE day is approximately bimodal, but in this case with a separation of only the sunny forest edges on the south facing slope, reflecting a considerably smaller number of pixels that exhibit sufficient early-season ablation to prepone peak SWE day relative to all other pixels.

Analogous to our approach in Section 3.3, we consider time series at point locations to unravel the process-level mechanisms that cause potential inconsistencies in snow cover descriptor patterns between years (Figure 10). To better highlight these inter-annual variations, we focus on a set of points located in semi-open conditions on the south-exposed slope, i.e., where they can potentially receive early-season direct shortwave radiation (locations see Supplementary Material, Figure S6.1). These include a point in a large gap, close to the south-facing canopy edge (yellow); a point in a smaller gap (dark red); and two points under relatively sparse canopy in a rather sunny (dark blue) and a shady (cyan) location, respectively. Due to the limited range in local canopy cover at these points, the differences in accumulation caused by interception are less pronounced than for the examples shown in Section 3.3 (c.f. Figure 10 vs. Figure 6). Yet, these points experience different drivers of ablation and therefore react differently to variations in meteorological conditions between the years.

Firstly, we note that accumulation patterns (i.e. peak SWE) vary between years based on the timing of the first ablation events relative to the timing of peak SWE, particularly whether or not considerable ablation events occur during the accumulation period (Figure 10a). In 2019, when all major snowfall events occur prior to the first melt episode, gaps feature the highest peak SWE, corresponding to low interception losses (yellow and red). In 2017 in contrast, overall accumulation is low, and substantial melt precedes the last major accumulation event, which is sufficient to cause melt-out at some of the most sun-exposed locations; peak SWE at the sunny canopy gap point (yellow) is now thus the lowest of the four points considered. It should be noted that for all WY's considered here, onset of full snow cover happened roughly simultaneously across the entire

model domain; early ablation events leading to partial melt-out prior of the onset of full snow cover (not shown, but observed e.g. in WY 2016) would obviously further complicate peak SWE patterns.

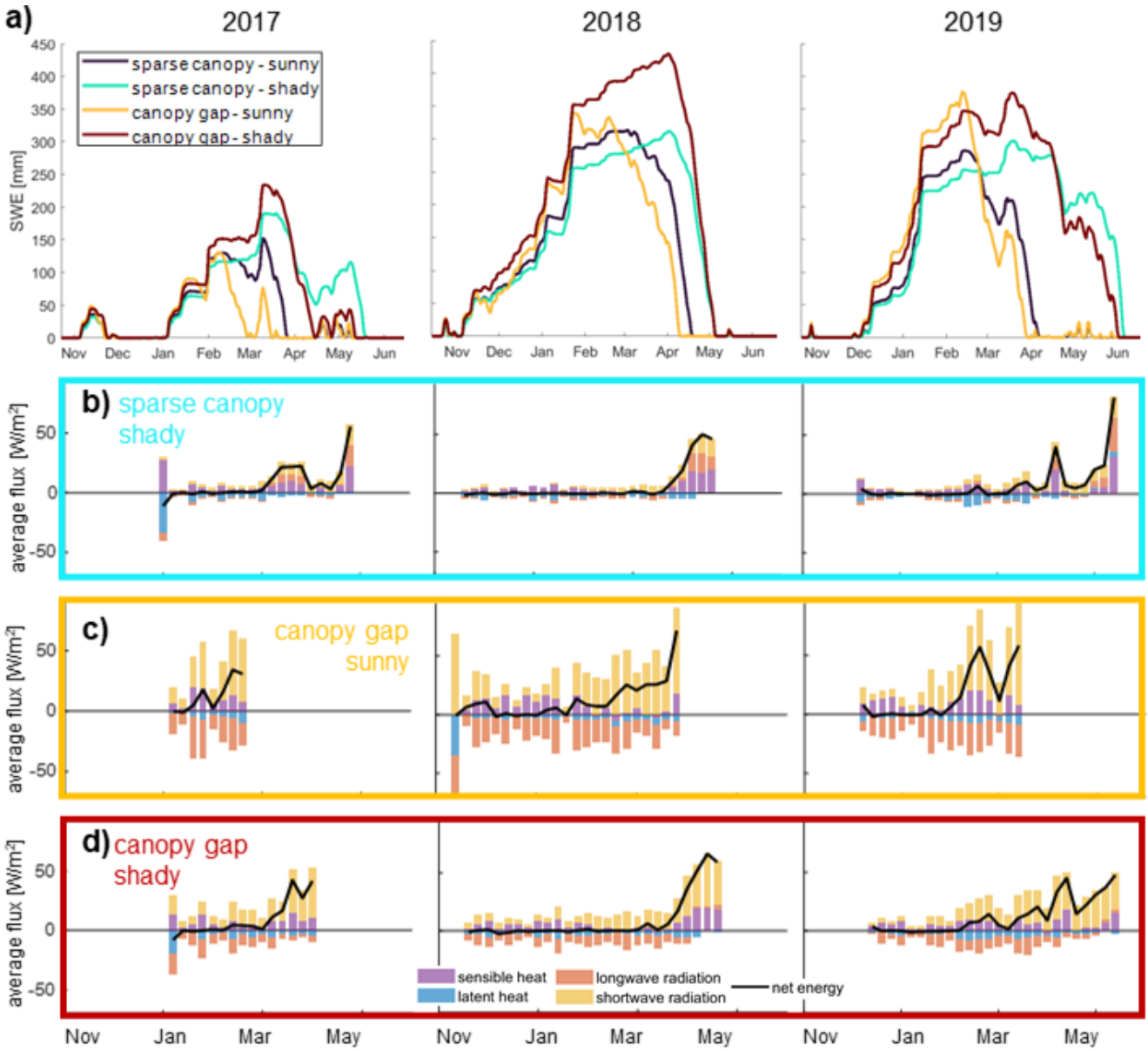

Figure 10: Impact of meteorological conditions illustrated by comparing three different WYs (columns), including (a) SWE evolution at four example points (locations see S3) and surface energy partitioning pathways at three of these, i.e. (b) a shady sparse canopy location, (c) a sunny canopy gap location, and (d) a shady canopy gap location.

Second, we note that the relative timing of snow disappearance between years can vary across the domain, based on the availability of melt energy over the course of the season (Figure 10a). Points that normally receive early-season shortwave irradiance (i.e., the dark blue and the yellow point) melt out later in WY 2018 compared to 2019 because less shortwave

irradiance is available in February (see strong positive shortwave contributions in Figure 10c). In contrast, points in shadier locations (cyan and red) melt earlier in WY 2018 because of the consistently warmer and sunnier weather in spring compared to 2019 (see earlier switch to both positive shortwave and longwave contributions in Figure 10b+d). The opposed effect of these differences in meteorological conditions causes snow disappearance day of the four points to be much closer in WY 2018 than in 2019. The overall melt-out patterns will thus vary between WYs, even if the dominating fluxes at each specific location remain approximately consistent (Figure 10b-d).

4 Discussion

4.1 Process-level insights

Spatio-temporal snow cover dynamics and associated snow accumulation and ablation patterns are a result of superimposed processes that themselves vary as a function of both time-invariant physiographic features (vegetation, topography) and time-varying meteorological conditions. While the phenological analysis of snow season descriptors presented in Sections 3.1-3.2 paints a complex picture of snow distribution patterns, the process-level analysis in Sections 3.3-3.5 allowed us to attribute the processes that underly these patterns. The main takeaway from this work is that patterns of snow season descriptors and their inter-seasonal consistency can only be explained by considering all three factors, canopy structure, topography, and meteorology, as well as their interaction throughout the snow season.

Snow distribution patterns at any point in time arise from an interplay between accumulation and ablation patterns. For the study site considered here, our analysis showed that snow cover dynamics result from the superposition of (1) a pattern that is temporally static and dependent on canopy structure alone, with more snow where there is less canopy (i.e., accumulation mostly controlled by interception) and (2) a time-varying pattern with complex dependencies on canopy structure, solar position, weather, and topography, with an overall tendency for faster ablation where there is less canopy (i.e., melt mostly controlled by shortwave radiation). Depending on the relative strength of each of both signals, three regimes of snow cover dynamics are principally possible:

R1. Snow distribution can be described as function of canopy structure alone throughout the whole season. This is the case when accumulation creates a strong signal, and ablation patterns are too homogeneous or too weak to override this signal, so that areas that accumulate less snow also melt out first.

R2. Snow accumulation patterns can be described as a function of canopy structure during the accumulation period, but those patterns will be overridden by ablation patterns during the ablation period. Consequently, snow disappearance date exhibits no simple relationship with canopy structure.

R3. Early-season ablation inhibits formation of simple snow accumulation patterns, and snow distribution patterns remain weakly correlated with canopy structure throughout the entire season.

Based on these regimes and using WY 2018 as an example, Figure 11c shows a conceptual subdivision of our model domain into 4 zones. Zone A does not feature early-season ablation and exhibits snow disappearance patterns that carry the imprint of

local canopy cover; Zone B is characterized by substantial cumulative early-season ablation amounts (Figure 11a); Zones C and D largely lack early ablation but exhibit fewer clear linkages between canopy cover and snow disappearance day (Figure 11b). Note that Zones C and D are treated separately due to elevational differences. As a crosscheck, we computed the temporal evolution of the correlation coefficient between SWE and local canopy cover for each of the four zones separately (Figure 11d). As expected, Zone A (R1) features a strong negative correlation between SWE and local canopy cover throughout the entire season; Zone D (R2) exhibits a similarly strong correlation at the beginning of the season which then degrades during ablation season; and Zone B (R3) a weaker correlation even early in the season, where each ablation episode degrades and each interception event improves the correlation, until the ablation season causes the correlation to collapse more permanently. Zone C seems to show characteristics of R2 in 2018, but of R3 in 2016, which implies that the regime found at a specific location may not be consistent from year to year.

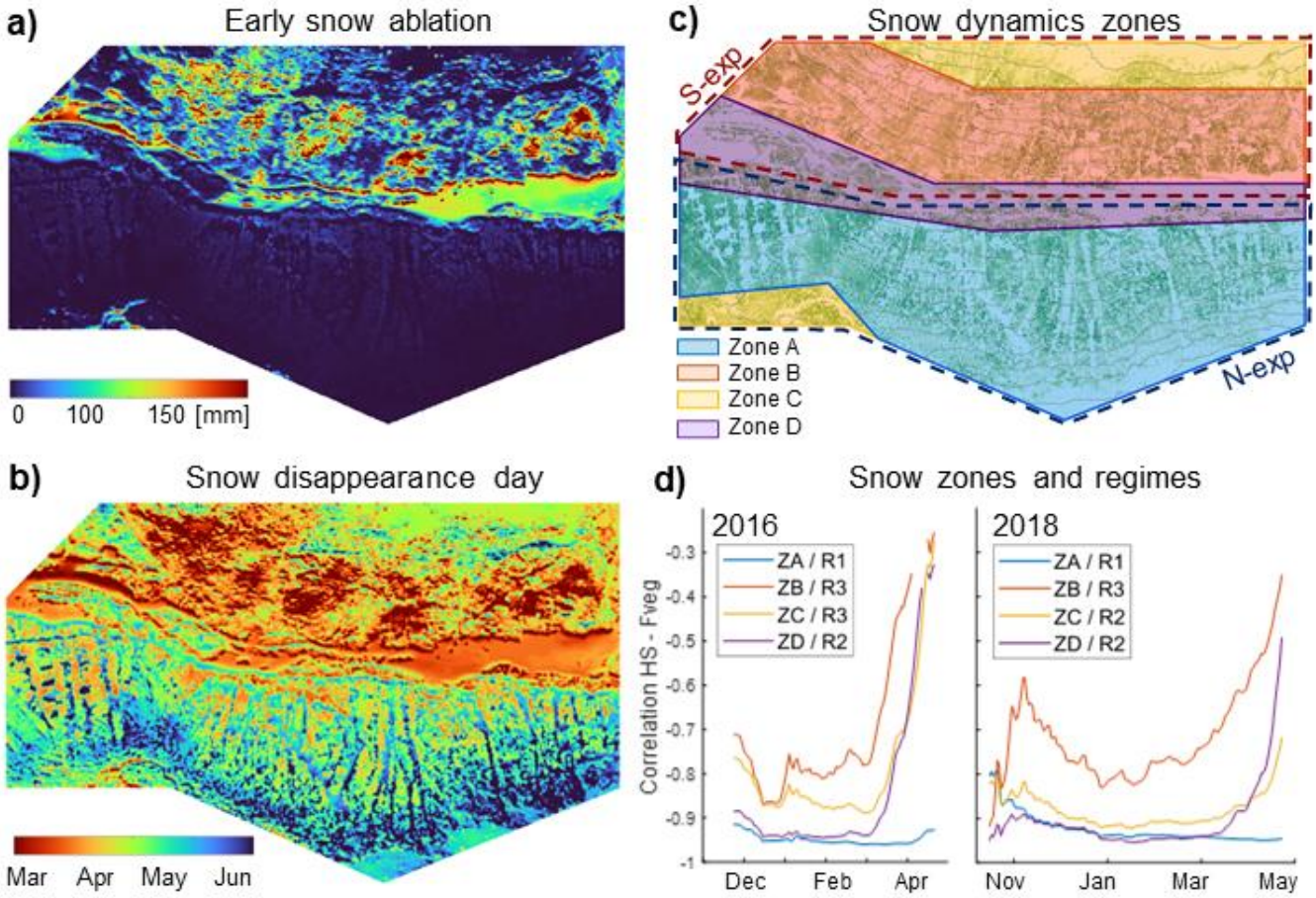

Figure 11: Conceptual subdivision of study domain into snow cover evolution regimes, the identification of which is based on maps of cumulative SWE ablation between mid-January and mid-March (a) and snow disappearance day (b) in WY 2018. Resulting zones (c) and evolution of the correlation coefficients between snow depth and vegetation cover fraction in these for WYs 2016 and 2018, resulting in the attribution to a specific regime (d).

The co-occurrence of different regimes across our study domain is a consequence of topography because early-season shortwave irradiance is a prerequisite for regime 3, while its absence is a prerequisite for regime 1. North-exposed slopes are prone to falling into regime 1, while south-exposed slopes tend to conform with regime 3. Regime 2 is less evident in our example, but most likely to be found in flat areas with large canopy gaps, where early-season ablation is not expected but substantial melt energy gradients can evolve during ablation. The impact of inter-annual variability in meteorological conditions can lead to the same locations hosting different regimes in different WYs: Differences result from either weaker accumulation patterns or variations in magnitude and timing of shortwave irradiance. This finding is in line with Lundquist and Flint (2006), who attributed variability in snowmelt patterns between years with early and late snowmelt onset to differences in topographic shading. Our analysis also furthers the conceptual framework presented by Lundquist et al. (2013). Based on site-scale simulations of the net radiative balance, they established timing of early melt, determined by the climatological temperature at a site, as the primary control of whether denser forest would generally accelerate or delay snowmelt through the prevalence of longwave radiation enhancement or shading, respectively. Our approach, involving more processes and detailed canopy structure information, confirms the importance of early-season ablation, but demonstrates the additional key role of shortwave radiation patterns in determining snow dynamics regimes at smaller spatial scales.

The categorization of snow cover dynamics into regimes provides a context to temporal snapshots of snow distribution patterns, such as those derived from singular LiDAR datasets. The temporal evolution of correlation coefficients (Figure 11d) corroborates findings from Koutantou et al. (2022), who used maps of modelled sub-canopy irradiance to explain why snow distribution patterns exhibited different dependencies on canopy structure at their north- and south-exposed survey sites. A decay of the correlation between snow distribution and canopy structure between two LiDAR acquisitions in spring was also observed by Mazzotti et al. (2019a) for sites with less topographic variability. In general, our process-level insights explain why these correlations can vary between years and regimes, as shown in this study, and hence why different studies may have observed different and sometimes inconsistent dependencies between snow and canopy variables, depending on when and where data were acquired (e.g. Safa et al., 2021; Currier and Lundquist, 2018).

4.2 Implications and applications

The process-level insights discussed in the previous section have important implications in a variety of contexts in which small-scale variability of forest snow cover dynamics is relevant. We elaborate on three such examples in the following.

Firstly, our findings indicate that strategies to account for sub-grid variability in coarser-resolution models that are intended for application to sub-alpine environments need to account for variations in canopy structure, topography, and meteorology. This is particularly the case at sub-kilometre model resolutions, where variability in driving meteorological conditions induced by topography is at least partially resolved (e.g., through temperature lapse rates and orographic precipitation gradients), while variability in snow cover dynamics caused by canopy structure occurs at much smaller spatial scales and needs to be parameterized (Clark et al., 2011). The south-exposed slope in our model domain featured stronger variability and more complex patterns of snow cover descriptors than the north-exposed slope, with impacts on the evolution of fractional snow-

covered area in grid cells that include such terrain. To our knowledge, sub-grid variability parametrizations that incorporate these effects are inexistent to date (Dickerson-Lange et al., 2015; Mazzotti et al., 2021; Schneider et al., 2020), but their development is a promising avenue for further model improvement. However, recent studies have suggested tiling schemes based on fine-scale canopy structure as an alternative approach to representing sub-grid variability (Broxton et al., 2021; Currier et al., 2022), in line with our findings.

Secondly, our simulations evidence a strong complexity in eco-hydrologically relevant processes across a still relatively limited study domain. The large range of snow cover durations observed creates spatial variability in ground insulating properties and soil temperatures. Snow water input to the ground also exhibits strong spatial heterogeneity due to variability in snow melt magnitudes and rates, with further influences on soil moisture evolution. As soil conditions control a wide range of biophysical processes (Neumann et al., 2019; Stark et al., 2020; Harpold, 2016), their spatial heterogeneity potentially implies strong variability of habitat characteristics across relatively small spatial scales (Niittynen et al., 2018). It is also possible that the observed process variability affects ecologically relevant snow properties such as surface layer density (Boelman et al., 2019; Gilbert et al., 2017) or the formation of ice layers in the snowpack (Rasmus et al., 2018). This is an unexplored research topic to date, as resolving these internal snowpack processes would require a more sophisticated snow scheme than available in FSM2. Coupling of detailed canopy representation to snow physics models such as Crocus (Vionnet et al., 2012; Lafaysse et al., 2017) and SNOWPACK (Bartelt and Lehning, 2002; Lehning et al., 2002; Gouttevin et al., 2015) would hence be a prerequisite. Overall, our results advocate that small-scale landscape heterogeneity needs to be considered when addressing snow-related eco-hydrological questions in sub-alpine forested environments.

Lastly, process-level insights allow us to extrapolate our findings spatially and temporally. While it is known that forest snow cover dynamics differ across climates (Lundquist et al., 2013; Dickerson-Lange et al., 2021; Safa et al., 2021), the same underlying processes are active everywhere. The snow distribution patterns found in this study may thus not be directly transferrable to other regions, but improved understanding of how physiographic and meteorological factors interact with one another allows us to better predict where and when certain processes will prevail. Consequently, we expect the prevalence of specific snow dynamics regimes to vary with latitude, regional temperature, and snowfall characteristics. Likewise, these insights enable improved prediction of how patterns may shift following environmental change. Our findings suggest, for instance, that canopy removal may have the opposite effect in different topographic locations, i.e., earlier and faster ablation on south-exposed slopes but longer snow retention in north-exposed ones. Warmer temperatures earlier in the season favour longwave-radiation driven ablation (Lundquist et al., 2013), shifting the relative timing of shortwave vs. longwave-radiation driven ablation. Such a shift which would likely accentuate accumulation patterns and thus alter melt-out patterns on south-exposed slopes but only show minor impacts on north-exposed slopes.

The use of hyper-resolution models in the context of forest management and climate change impact studies is still underexploited but should be encouraged in the future as only process-based models allow predictions that extrapolate from currently known conditions. Indeed, forest snowpacks in sub-alpine regions reside at climate-sensitive elevations (Schöner et

al., 2019; Pepin et al., 2015), and forest structural change is widely and rapidly happening (Albrich et al., 2020; Goeking and Tarboton, 2020).

4.3 Assets, limitations, and outlook

Considerations in Sections 4.1 and 4.2 underline the assets of a process-based modelling approach in terms of its capabilities to resolve individual process dynamics. Additionally, modelling allowed us to obtain spatially and temporally continuous information, which is not feasible with today's observation technology. Most ALS-based snow datasets that cover large areas are available for only a few temporal snapshots (Safa et al., 2021; Currier and Lundquist, 2018; Harpold et al., 2014; Broxton et al., 2019), while existing attempts to acquire snow distribution time series are very limited in spatial extent and mostly cover one winter season only (Koutantou et al., 2022; Broxton and van Leeuwen, 2020). Process-level data that is both spatially and temporally explicit is even more scarce and extremely challenging to obtain (Moeser et al., 2015; Malle et al., 2019, 2021; Mazzotti et al., 2019b). Model application, in contrast, is only limited by the availability of driving meteorological data and surface datasets, and thus potentially applicable to extensive spatial and temporal domains.

Modelled process dynamics, however, can only yield satisfactory estimates of reality if the model representations of the processes involved are sufficiently accurate. For this study, we used FSM2, which we believe to be particularly suited given previous validation efforts demonstrating the model's capability to accurately represent individual processes related to the snowpack surface energy balance (Mazzotti et al. 2020a). Yet, we acknowledge that our findings depend on modelling choices and results might vary when using alternative models or process parametrizations. Therefore~~While models like FSM2 already enable tackling relevant research questions~~, the modelling community should strive for continued improvement. On one hand, the representation of some processes could still be improved, and associated uncertainties should be evaluated systematically across the full range of canopy structure and topographic diversity of the application domains of interest. This is especially the case for processes involving snow in the canopy (Lundquist et al., 2021; Lumbrazo et al., 2022). Moreover, while Mazzotti et al. (2020a) could infer spatial patterns of snow surface fluxes from their data, direct validation of turbulent fluxes is challenging even with recent measurement techniques (see e.g., Conway et al., 2018; Peltola et al., 2020; Haugeneder et al., 2022).

Some processes, such as snow transport by wind and gravitational redistribution by avalanches in steep slopes, are not represented in the model framework used here. These processes significantly drive snow distribution patterns in open alpine terrain but are assumed to have a smaller impact on fine-scale patterns in forests. Efforts to couple FSM2 to snow redistribution models (e.g., Liston and Sturm, 1999; Bernhardt and Schulz, 2010) are ongoing. Additionally, mass and energy exchange between neighbouring locations may become relevant at hyper-resolutions (Schlögl et al., 2018), and lateral coupling would likely improve the representation of expanding snow-free areas in spring. Coupling to a soil or eco-hydrological model (Fatichi et al., 2012; Tague and Band, 2004) would further extend the potential applications of hyper-resolution forest snow schemes beyond just snow cover dynamics. Finally, a major challenge concerns the estimation of model parameters that are potentially variable in space. This approach was not pursued in this study but has been shown to considerably increase the benefits of

calibration efforts (Wrzesien et al., 2022). Approaches to automate model calibration across the full range of canopy structures and topographic settings may thus further improve the skill of models like FSM2.

In the longer term, combining hyper-resolution models and observations to leverage their complementary assets is likely the most promising avenue to advance our understanding of forest snow cover dynamics in complex terrain. Plausibility checks as presented in Section 2.3 are indispensable for the verification of model use cases, as well as for continued model enhancement and refinement, and there is potential for improvement here as well. For instance, the use of RGB satellite data to validate melt-out patterns (Section 2.3) is promising despite limited visibility of snow under the canopy. Automated algorithms to extract snow cover information from RGB imagery are not currently applicable to forested complex terrain (Deschamps-Berger et al., 2020; Gascoin et al., 2019), but would encourage the use of such datasets for this purpose. If respective workflows are continuously improved, enabling simulations and observations to be used in tandem and to benefit from each other (e.g., through data assimilation approaches), hyper-resolution model applications at large temporal and spatial scales in the contexts discussed in Section 4.2 promise advances in eco-hydrological and land surface modelling research.

5 Conclusion

This study represents the first multi-year application of a hyper-resolution forest snow model capable of resolving tree-scale processes within a sub-alpine valley, aimed at investigating how snow cover dynamics and the underlying processes are shaped by the interplay of (1) canopy structure, (2) terrain, and (3) meteorological conditions. The chosen approach yielded process-level insights that could not be obtained based on snow distribution datasets alone.

Our findings evidenced that all these three factors must be considered when attempting to explain spatio-temporal snow cover dynamics. Canopy structure exerts the primary control on accumulation patterns, yet the resulting snow distribution can be disrupted by ablation patterns, which are primarily driven by the distribution of shortwave radiation. Because shortwave radiation exhibits complex canopy dependencies and tends to counteract accumulation patterns, it is the timing of radiation relative to the strength of the accumulation patterns that determines whether accumulation patterns persist until melt-out, or whether they are overridden by more complex ablation patterns. Since amount and timing of shortwave irradiance are largely controlled by topography, south-exposed slopes are more prone to accumulation patterns being superseded by ablation patterns even early in the season compared to north-exposed slopes, where accumulation patterns likely persist throughout melt-out. Finally, variability in meteorological conditions alters the relative strength of processes (accumulation, direct insolation, longwave driven ablation) and can thus cause snow accumulation and ablation pattern inconsistencies between years. This framework explains why snow distribution patterns in some areas exhibit a strong relationship with canopy structure, while they do not in other areas, and why this can change between years.

Process understanding gained from this work provides context to existing snow distribution datasets and a proof of concept for the continued development and application of hyper-resolution modelling approaches to forest-snow related research in complex terrain. Potential usages include questions that revolve around developing sub-grid variability parametrization in

coarse-resolution models, exploring the eco-hydrological effects of the observed small-scale snow dynamics, and the application of hyper-resolution models in environmental change impact studies.

Data and code availability. The FSM2 model code is available on GitHub under https://github.com/GiuliaMazzotti/FSM2/tree/hyres_enhanced_canopy, release FSM2.0.3. Model input datasets are available on WSL's data repository EnviDat (doi:10.16904/envidat.338).

Author contributions. GM and TJ designed the study. CW did the radiation modelling and provided canopy structure input datasets for FSM2. LQ and BC contributed to the development of the model framework and the preparation of meteorological input data. GM performed FSM2 simulations and analysed the results, with input from TJ. GM wrote the manuscript, with feedback from all authors.

Competing interests. The authors declare that they have no conflict of interests.

Acknowledgements. This study was partly funded by the WSL Institute for Snow and Avalanche Research SLF and by the Swiss Federal Office for the Environment (FOEN). Part of this work was carried out at the Centre des Études de la Neige (MétéoFrance, CNRM) under SNSF Postdoc.Mobility grant P500PN_202741. We would like to thank Kalliopi Koutantou for providing UAV-LiDAR data and for many informal chats during fieldwork, which sparked the idea for this research. We thank Christian Ginzler for giving us access to Planetscope data. We are grateful to Rebecca Mott and Jan Magnusson from the Operational Snow Hydrological Service at SLF for their support on matters related to the meteorological input and the model framework and to Richard Essery for his help with FSM2-related questions. We appreciated numerous scientific discussions with, Matthieu Lafaysse and Jari-Pekka Nousu while this work was taking shape. ~~Finally, we~~We would further like to thank Jessica Lundquist, Joschka Geissler, ~~and~~ an anonymous reviewer, and the Editor, Jan Seibert, for their comments ~~on the discussion paper~~ which helped improve the original manuscript. Finally, GM gratefully acknowledges the EGU Virtual Outstanding Student and PhD candidate Presentation Award 2021 that supported the publication of this article.

References

Albrich, K., Rammer, W., and Seidl, R.: Climate change causes critical transitions and irreversible alterations of mountain forests, Global Change Biology, 26, 4013–4027, https://doi.org/10.1111/gcb.15118, 2020.

Barnhart, T. B., Molotch, N. P., Livneh, B., Harpold, A. A., Knowles, J. F., and Schneider, D.: Snowmelt rate dictates streamflow: Snowmelt Rate Dictates Streamflow, Geophys. Res. Lett., 43, 8006–8016, https://doi.org/10.1002/2016GL069690, 2016.

Bartelt, P. and Lehning, M.: A physical SNOWPACK model for the Swiss avalanche warning Part I: numerical model, Cold Regions Science and Technology, 23, 2002.

Bebi, P., Seidl, R., Motta, R., Fuhr, M., Firm, D., Krumm, F., Conedera, M., Ginzler, C., Wohlgemuth, T., and Kulakowski, D.: Changes of forest cover and disturbance regimes in the mountain forests of the Alps, For Ecol Manage, 388, 43–56, https://doi.org/10.1016/j.foreco.2016.10.028, 2017.

Bernhardt, M., and Schultz, K.: SnowSlide: A simple routine for calculating gravitational snow transport, Geophysical Research Letters, 37(11), doi:10.1029/2010GL043086, 2010.

Boelman, N. T., Liston, G. E., Gurarie, E., Meddens, A. J. H., Mahoney, P. J., Kirchner, P. B., Bohrer, G., Brinkman, T. J., Cosgrove, C. L., Eitel, J. U. H., Hebblewhite, M., Kimball, J. S., LaPoint, S., Nolin, A. W., Pedersen, S. H., Prugh, L. R., Reinking, A. K., and Vierling, L. A.: Integrating snow science and wildlife ecology in Arctic-boreal North America, Environ. Res. Lett., 14, 010401, https://doi.org/10.1088/1748-9326/aaeec1, 2019.

Bormann, K. J., Brown, R. D., Derksen, C., and Painter, T. H.: Estimating snow-cover trends from space, Nature Climate Change, 8, 924–928, https://doi.org/10.1038/s41558-018-0318-3, 2018.

Broxton, P. D. and van Leeuwen, W. J. D.: Structure from Motion of Multi-Angle RPAS Imagery Complements Larger-Scale Airborne Lidar Data for Cost-Effective Snow Monitoring in Mountain Forests, Remote Sensing, 12, 2311, https://doi.org/10.3390/rs12142311, 2020.

Broxton, P. D., Harpold, A. A., Biederman, J. A., Troch, P. A., Molotch, N. P., and Brooks, P. D.: Quantifying the effects of vegetation structure on snow accumulation and ablation in mixed-conifer forests, Ecohydrol., 8, 1073–1094, https://doi.org/10.1002/eco.1565, 2015.

Broxton, P. D., Leeuwen, W. J. D., and Biederman, J. A.: Improving Snow Water Equivalent Maps With Machine Learning of Snow Survey and Lidar Measurements, Water Resour. Res., 55, 3739–3757, https://doi.org/10.1029/2018WR024146, 2019.

Broxton, P. D., Leeuwen, W. J. D., and Biederman, J. A.: Forest cover and topography regulate the thin, ephemeral snowpacks of the semiarid Southwest United States, Ecohydrology, 13, https://doi.org/10.1002/eco.2202, 2020.

Broxton, P. D., Moeser, C. D., and Harpold, A.: Accounting for Fine-Scale Forest Structure is Necessary to Model Snowpack Mass and Energy Budgets in Montane Forests, Water Resources Research, 57, e2021WR029716, https://doi.org/10.1029/2021WR029716, 2021.

Conway, J.P., Pomeroy, J. W., Helgason, W. D., Kinar, N. J., Challenges in Modeling Turbulent Heat Fluxes to Snowpacks in Forest Clearings, Journal of Hydrometeorology, 19, 1599-1616, https://doi.org/10.1175/JHM-D-18-0050.1, 2018.

Currier, W. R. and Lundquist, J. D.: Snow Depth Variability at the Forest Edge in Multiple Climates in the Western United States, Water Resour. Res., 54, 8756–8773, https://doi.org/10.1029/2018WR022553, 2018.

Currier, W. R., Pflug, J., Mazzotti, G., Jonas, T., Deems, J. S., Bormann, K. J., Painter, T. H., Hiemstra, C. A., Gelvin, A., Uhlmann, Z., Spaete, L., Glenn, N. F., and Lundquist, J. D.: Comparing Aerial Lidar Observations With Terrestrial Lidar and Snow-Probe Transects From NASA's 2017 SnowEx Campaign, Water Resources Research, 55, 6285-6294, https://doi.org/10.1029/2018WR024533, 2019.

Currier, W. R., Sun, N., Wigmosta, M., Cristea, N., and Lundquist, J. D.: The impact of forest-controlled snow variability on late-season streamflow varies by climatic region and forest structure, Hydrological Processes, 36, e14614, https://doi.org/10.1002/hyp.14614, 2022.

Deschamps-Berger, C., Gascoin, S., Berthier, E., Deems, J., Gutmann, E., Dehecq, A., Shean, D., and Dumont, M.: Snow depth mapping from stereo satellite imagery in mountainous terrain: evaluation using airborne laser-scanning data, The Cryosphere, 14, 2925–2940, https://doi.org/10.5194/tc-14-2925-2020, 2020.

Dickerson-Lange, S. E., Lutz, J. A., Gersonde, R., Martin, K. A., Forsyth, J. E., and Lundquist, J. D.: Observations of distributed snow depth and snow duration within diverse forest structures in a maritime mountain watershed, Water Resour. Res., 51, 9353–9366, https://doi.org/10.1002/2015WR017873, 2015.

Dickerson-Lange, S. E., Vano, J. A., Gersonde, R., and Lundquist, J. D.: Ranking Forest Effects on Snow Storage: A Decision Tool for Forest Management, Water Resources Research, 57, e2020WR027926, https://doi.org/10.1029/2020WR027926, 2021.

Ellis, C. R., Pomeroy, J. W., Essery, R. L. H., and Link, T. E.: Effects of needleleaf forest cover on radiation and snowmelt dynamics in the Canadian Rocky Mountains, Can. J. For. Res., 41, 608–620, https://doi.org/10.1139/X10-227, 2011.

Essery, R.: A factorial snowpack model (FSM 1.0), Geoscientific Model Development, 8, 3867–3876, https://doi.org/10.5194/gmd-8-3867-2015, 2015.

Fatichi, S., Ivanov, V. Y., and Caporali, E.: A mechanistic ecohydrological model to investigate complex interactions in cold and warm water-controlled environments: 2. Spatiotemporal analyses, Journal of Advances in Modeling Earth Systems, 4, https://doi.org/10.1029/2011MS000087, 2012.

Gascoin, S., Grizonnet, M., Bouchet, M., Salgues, G., and Hagolle, O.: Theia Snow collection: high-resolution operational snow cover maps from Sentinel-2 and Landsat-8 data, Earth System Science Data, 11, 493–514, https://doi.org/10.5194/essd-11-493-2019, 2019.

Gilbert, S. L., Hundertmark, K. J., Person, D. K., Lindberg, M. S., and Boyce, M. S.: Behavioral plasticity in a variable environment: snow depth and habitat interactions drive deer movement in winter, Journal of Mammalogy, 98, 246–259, https://doi.org/10.1093/jmammal/gyw167, 2017.

Goeking, S. A. and Tarboton, D. G.: Forests and Water Yield: A Synthesis of Disturbance Effects on Streamflow and Snowpack in Western Coniferous Forests, Journal of Forestry, 118, 172–192, https://doi.org/10.1093/jofore/fvz069, 2020.

Gouttevin, I., Lehning, M., Jonas, T., Gustafsson, D., and Mölder, M.: A two-layer canopy model with thermal inertia for an improved snowpack energy balance below needleleaf forest (model SNOWPACK, version 3.2.1, revision 741), Geosci. Model Dev., 8, 2379–2398, https://doi.org/10.5194/gmd-8-2379-2015, 2015.

Griessinger, N., Schirmer, M., Helbig, N., Winstral, A., Michel, A., and Jonas, T.: Implications of observation-enhanced energy-balance snowmelt simulations for runoff modeling of Alpine catchments, Advances in Water Resources, 133, 103410, https://doi.org/10.1016/j.advwatres.2019.103410, 2019.

Günther, D., Marke, T., Essery, R., and Strasser, U.: Uncertainties in Snowpack Simulations—Assessing the Impact of Model Structure, Parameter Choice, and Forcing Data Error on Point-Scale Energy Balance Snow Model Performance, Water Resources Research, 55, 2779-2800, https://doi.org/10.1029/2018WR023403, 2019.

Harpold, A. A.: Diverging sensitivity of soil water stress to changing snowmelt timing in the Western U.S., Advances in Water Resources, 92, 116–129, https://doi.org/10.1016/j.advwatres.2016.03.017, 2016.

Harpold, A. A., Guo, Q., Molotch, N., Brooks, P. D., Bales, R., Fernandez-Diaz, J. C., Musselman, K. N., Swetnam, T. L., Kirchner, P., Meadows, M. W., Flanagan, J., and Lucas, R.: LiDAR-derived snowpack data sets from mixed conifer forests across the Western United States, Water Resour. Res., 50, 2749–2755, https://doi.org/10.1002/2013WR013935, 2014.

Harpold, A. A., Krogh, S. A., Kohler, M., Eckberg, D., Greenberg, J., Sterle, G., and Broxton, P. D.: Increasing the efficacy of forest thinning for snow using high-resolution modeling: A proof of concept in the Lake Tahoe Basin, California, USA, Ecohydrology, 13, https://doi.org/10.1002/eco.2203, 2020.

Haugeneder, M., Lehning, M., Reynolds, D., Jonas, T., and Mott, R.: A Novel Method to Quantify Near-Surface Boundary-Layer Dynamics at Ultra-High Spatio-Temporal Resolution, Boundary-Layer Meterology, https://doi.org/10.1007/s10546-022-00752-3, 2022.

Jonas, T., Webster, C., Mazzotti, G., and Malle, J.: HPEval: A canopy shortwave radiation transmission model using high-resolution hemispherical images, Agricultural and Forest Meteorology, 284, 107903, https://doi.org/10.1016/j.agrformet.2020.107903, 2020.

Khosravipour, A., Skidmore, A. K., Isenburg, M., Wang, T., and Hussin, Y. A.: Generating Pit-free Canopy Height Models from Airborne Lidar, photogramm eng remote sensing, 80, 863–872, https://doi.org/10.14358/PERS.80.9.863, 2014.

Koutantou, K., Mazzotti, G., Brunner, P., Webster, C., and Jonas, T.: Exploring snow distribution dynamics in steep forested slopes with UAV-borne LiDAR, Cold Regions Science and Technology, 200, 103587, https://doi.org/10.1016/j.coldregions.2022.103587, 2022.

Krogh, S. A., Broxton, P. D., Manley, P. N., and Harpold, A. A.: Using Process Based Snow Modeling and Lidar to Predict the Effects of Forest Thinning on the Northern Sierra Nevada Snowpack, Front. For. Glob. Change, 3, 21, https://doi.org/10.3389/ffgc.2020.00021, 2020.

Lafaysse, M., Cluzet, B., Dumont, M., Lejeune, Y., Vionnet, V., and Morin, S.: A multiphysical ensemble system of numerical snow modelling, The Cryosphere, 11, 1173–1198, https://doi.org/10.5194/tc-11-1173-2017, 2017.

Lawler, R. R. and Link, T. E.: Quantification of incoming all-wave radiation in discontinuous forest canopies with application to snowmelt prediction, Hydrol. Process., 25, 3322–3331, https://doi.org/10.1002/hyp.8150, 2011.

Lehning, M., Bartelt, P., Brown, B., Fierz, C., and Satyawali, P.: A physical SNOWPACK model for the Swiss avalanche warning Part II. Snow microstructure, Cold Regions Science and Technology, 21, 2002.

Liston G. E., and Sturm, M.: A snow-transport model for complex terrain, Journal of Glaciology, 44(148), 498-516, https://doi.org/10.3189/S0022143000002021, 1999.

Lumbrazo, C., Bennett, A., Currier, W. R., Nijssen, B., and Lundquist, J.: Evaluating Multiple Canopy-Snow Unloading Parameterizations in SUMMA With Time-Lapse Photography Characterized by Citizen Scientists, Water Resources Research, 58, e2021WR030852, https://doi.org/10.1029/2021WR030852, 2022.

Lundquist, J. D., and Flint, A. L.: Onset of Snowmelt and Streamflow in 2004 in the Western United States: How Shading May Affect Spring Streamflow Timing in a Warmer World, Journal of Hydrometeorology, 7(6), 1199-1217, https://doi.org/10.1175/JHM539.1, 2006.

Lundquist, J. D., Dickerson-Lange, S. E., Lutz, J. A., and Cristea, N. C.: Lower forest density enhances snow retention in regions with warmer winters: A global framework developed from plot-scale observations and modeling: Forests and Snow Retention, Water Resour. Res., 49, 6356–6370, https://doi.org/10.1002/wrcr.20504, 2013.

Lundquist, J. D., Dickerson-Lange, S., Gutmann, E., Jonas, T., Lumbrazo, C., and Reynolds, D.: Snow interception modelling: Isolated observations have led to many land surface models lacking appropriate temperature sensitivities, Hydrological Processes, 35, e14274, https://doi.org/10.1002/hyp.14274, 2021.

Malle, J., Rutter, N., Mazzotti, G., and Jonas, T.: Shading by Trees and Fractional Snow Cover Control the Subcanopy Radiation Budget, Journal of Geophysical Research: Atmospheres, 124, 3195–3207, https://doi.org/10.1029/2018JD029908, 2019.

Malle, J., Rutter, N., Webster, C., Mazzotti, G., Wake, L., and Jonas, T.: Effect of Forest Canopy Structure on Wintertime Land Surface Albedo: Evaluating CLM5 Simulations With In-Situ Measurements, Journal of Geophysical Research: Atmospheres, 126, e2020JD034118, https://doi.org/10.1029/2020JD034118, 2021.

Manninen, T. and Jääskeläinen, E.: The Effect of Boreal Forest Canopy on Snow Covered Terrain Broadband Albedo, 21, 2018.

Manning, A. L., Harpold, A., and Csank, A.: Spruce Beetle Outbreak Increases Streamflow From Snow-Dominated Basins in Southwest Colorado, USA, Water Resources Research, 58, e2021WR029964, https://doi.org/10.1029/2021WR029964, 2022.

Marty, C., Tilg, A.-M., and Jonas, T.: Recent Evidence of Large-Scale Receding Snow Water Equivalents in the European Alps, Journal of Hydrometeorology, 18, 1021–1031, https://doi.org/10.1175/JHM-D-16-0188.1, 2017.

Mazzotti, G., Currier, W. R., Deems, J. S., Pflug, J. M., Lundquist, J. D., and Jonas, T.: Revisiting Snow Cover Variability and Canopy Structure Within Forest Stands: Insights From Airborne Lidar Data, Water Resources Research, 55, 6198–6216, https://doi.org/10.1029/2019WR024898, 2019a.

Mazzotti, G., Malle, J., Barr, S., and Jonas, T.: Spatially Continuous Characterization of Forest Canopy Structure and Subcanopy Irradiance Derived from Handheld Radiometer Surveys, Journal of Hydrometeorology, 20, 1417–1433, https://doi.org/10.1175/JHM-D-18-0158.1, 2019b.

Mazzotti, G., Essery, R., Webster, C., Malle, J., and Jonas, T.: Process-Level Evaluation of a Hyper-Resolution Forest Snow Model Using Distributed Multisensor Observations, Water Resources Research, 56, e2020WR027572, https://doi.org/10.1029/2020WR027572, 2020a.

Mazzotti, G., Essery, R., Moeser, C. D., and Jonas, T.: Resolving Small-Scale Forest Snow Patterns Using an Energy Balance Snow Model With a One-Layer Canopy, Water Resources Research, 56, e2019WR026129, https://doi.org/10.1029/2019WR026129, 2020b.

Mazzotti, G., Webster, C., Essery, R., and Jonas, T.: Increasing the Physical Representation of Forest-Snow Processes in Coarse-Resolution Models: Lessons Learned From Upscaling Hyper-Resolution Simulations, Water Resources Research, 57, e2020WR029064, https://doi.org/10.1029/2020WR029064, 2021.

Moeser, C. D., Broxton, P. D., Harpold, A., and Robertson, A.: Estimating the Effects of Forest Structure Changes From Wildfire on Snow Water Resources Under Varying Meteorological Conditions, Water Resources Research, 56, e2020WR027071, https://doi.org/10.1029/2020WR027071, 2020.

Moeser, D., Roubinek, J., Schleppi, P., Morsdorf, F., and Jonas, T.: Canopy closure, LAI and radiation transfer from airborne LiDAR synthetic images, Agricultural and Forest Meteorology, 197, 158–168, https://doi.org/10.1016/j.agrformet.2014.06.008, 2014.

Moeser, D., Stähli, M., and Jonas, T.: Improved snow interception modeling using canopy parameters derived from airborne LiDAR data, Water Resour. Res., 51, 5041–5059, https://doi.org/10.1002/2014WR016724, 2015.

Mote, P. W., Li, S., Lettenmaier, D. P., Xiao, M., and Engel, R.: Dramatic declines in snowpack in the western US, npj Climate and Atmospheric Science, 1, 1–6, https://doi.org/10.1038/s41612-018-0012-1, 2018.

Neumann, R. B., Moorberg, C. J., Lundquist, J. D., Turner, J. C., Waldrop, M. P., McFarland, J. W., Euskirchen, E. S., Edgar, C. W., and Turetsky, M. R.: Warming Effects of Spring Rainfall Increase Methane Emissions From Thawing Permafrost, Geophysical Research Letters, 46, 1393–1401, https://doi.org/10.1029/2018GL081274, 2019.

Niittynen, P., Heikkinen, R. K., and Luoto, M.: Snow cover is a neglected driver of Arctic biodiversity loss, Nature Climate Change, 8, 997–1001, https://doi.org/10.1038/s41558-018-0311-x, 2018.

Niittynen, P., Heikkinen, R. K., Aalto, J., Guisan, A., Kemppinen, J., and Luoto, M.: Fine-scale tundra vegetation patterns are strongly related to winter thermal conditions, Nature Climate Change, 1–6, https://doi.org/10.1038/s41558-020-00916-4, 2020.

Notarnicola, C.: Hotspots of snow cover changes in global mountain regions over 2000–2018, Remote Sensing of Environment, 243, 111781, https://doi.org/10.1016/j.rse.2020.111781, 2020.

Painter, T. H., Berisford, D. F., Boardman, J. W., Bormann, K. J., Deems, J. S., Gehrke, F., Hedrick, A., Joyce, M., Laidlaw, R., Marks, D., Mattmann, C., McGurk, B., Ramirez, P., Richardson, M., Skiles, S. M., Seidel, F. C., and Winstral, A.: The Airborne Snow Observatory: Fusion of scanning lidar, imaging spectrometer, and physically-based modeling for mapping snow water equivalent and snow albedo, Remote Sensing of Environment, 184, 139–152, https://doi.org/10.1016/j.rse.2016.06.018, 2016.

Peltola, O., Lapo, K., Martinkauppi, I., O'Connor, E., Thomas, C. K., and Vesala, T.: Suitability of fibre-optic distributed temperature sensing for revealing mixing processes and higher-order moments at the forest–air interface, Atmospheric Measurement Techniques, 14, 2409-2427, https://doi.org/10.5194/amt-14-2409-2021, 2021.

Pepin, N., Bradley, R. S., Diaz, H. F., Baraer, M., Caceres, E. B., Forsythe, N., Fowler, H., Greenwood, G., Hashmi, M. Z., Liu, X. D., Miller, J. R., Ning, L., Ohmura, A., Palazzi, E., Rangwala, I., Schöner, W., Severskiy, I., Shahgedanova, M., Wang, M. B., Williamson, S. N., Yang, D. Q., and Mountain Research Initiative EDW Working Group: Elevation-dependent warming in mountain regions of the world, Nature Climate Change, 5, 424–430, https://doi.org/10.1038/nclimate2563, 2015.

Pflug, J. M. and Lundquist, J. D.: Inferring Distributed Snow Depth by Leveraging Snow Pattern Repeatability: Investigation Using 47 Lidar Observations in the Tuolumne Watershed, Sierra Nevada, California, Water Resources Research, 56, e2020WR027243, https://doi.org/10.1029/2020WR027243, 2020.

Raleigh, M., Lundquist, J. D., and Clark, M. P.: Exploring the impact of forcing error characteristics on physically based snow simulations within a global sensitivity analysis framework, Hydrology and Earth System Sciences, 19, 3153-3179, https://doi.org/10.5194/hess-19-3153-2015, 2015.

Rasmus, S., Kivinen, S., and Irannezhad, M.: Basal ice formation in snow cover in Northern Finland between 1948 and 2016, Environ. Res. Lett., 13, 114009, https://doi.org/10.1088/1748-9326/aae541, 2018.

Roth, T. R. and Nolin, A. W.: Characterizing Maritime Snow Canopy Interception in Forested Mountains, Water Resour. Res., 2018WR024089, https://doi.org/10.1029/2018WR024089, 2019.

Safa, H., Krogh, S. A., Greenberg, J., Kostadinov, T. S., and Harpold, A. A.: Unraveling the Controls on Snow Disappearance in Montane Conifer Forests Using Multi-Site Lidar, Water Resources Research, 57, e2020WR027522, https://doi.org/10.1029/2020WR027522, 2021.

Schirmer, M., and Pomeroy, J. W.: Processes governing snow ablation in alpine terrain – detailed measurements from the Canadian Rockies, Hydrology and Earth System Sciences, 24, 143-157, https://doi.org/10.5194/hess-24-143-2020, 2020.

Schlögl, S., Lehning, M., and Mott, R.: How Are Turbulent Sensible Heat Fluxes and Snow Melt Rates Affected by a Changing Snow Cover Fraction?, Frontiers in Earth Science, 6, 2018.

Schneider, D., Molotch, N. P., Deems, J. S., and Painter, T. H.: Analysis of topographic controls on depletion curves derived from airborne lidar snow depth data, Hydrology Research, 52, 253–265, https://doi.org/10.2166/nh.2020.267, 2020.

Schöner, W., Koch, R., Matulla, C., Marty, C., and Tilg, A.-M.: Spatiotemporal patterns of snow depth within the Swiss-Austrian Alps for the past half century (1961 to 2012) and linkages to climate change, International Journal of Climatology, 39, 1589–1603, https://doi.org/10.1002/joc.5902, 2019.

Seidl, R., Thom, D., Kautz, M., Martin-Benito, D., Peltoniemi, M., Vacchiano, G., Wild, J., Ascoli, D., Petr, M., Honkaniemi, J., Lexer, M. J., Trotsiuk, V., Mairota, P., Svoboda, M., Fabrika, M., Nagel, T. A., and Reyer, C. P. O.: Forest disturbances under climate change, Nature Climate Change, 7, 395–402, https://doi.org/10.1038/nclimate3303, 2017.

Seyednasrollah, B. and Kumar, M.: How Surface Radiation on Forested Snowpack Changes across a Latitudinal Gradient, Hydrology, 6, 62, https://doi.org/10.3390/hydrology6030062, 2019.

Siirila-Woodburn, E. R., Rhoades, A. M., Hatchett, B. J., Huning, L. S., Szinai, J., Tague, C., Nico, P. S., Feldman, D. R., Jones, A. D., Collins, W. D., and Kaatz, L.: A low-to-no snow future and its impacts on water resources in the western United States, Nat Rev Earth Environ, 2, 800–819, https://doi.org/10.1038/s43017-021-00219-y, 2021.

Stark, S., Martz, F., Ovaskainen, A., Vuosku, J., Männistö, M. K., and Rautio, P.: Ice-on-snow and compacted and absent snowpack exert contrasting effects on soil carbon cycling in a northern boreal forest, Soil Biology and Biochemistry, 150, 107983, https://doi.org/10.1016/j.soilbio.2020.107983, 2020.

Strasser, U., Warscher, M., and Liston, G. E.: Modeling Snow–Canopy Processes on an Idealized Mountain, Journal of Hydrometeorology, 12, 663–677, https://doi.org/10.1175/2011JHM1344.1, 2011.

Sturm, M., Goldstein, M. A., and Parr, C.: Water and life from snow: A trillion dollar science question, Water Resources Research, 53, 3534–3544, https://doi.org/10.1002/2017WR020840, 2017.

Tague, C. L. and Band, L. E.: RHESSys: Regional Hydro-Ecologic Simulation System—An Object-Oriented Approach to Spatially Distributed Modeling of Carbon, Water, and Nutrient Cycling, Earth Interactions, 8, 1–42, https://doi.org/10.1175/1087-3562(2004)8<1:RRHSSO>2.0.CO;2, 2004.

Vionnet, V., Brun, E., Morin, S., Boone, A., Faroux, S., Le Moigne, P., Martin, E., and Willemet, J.-M.: The detailed snowpack scheme Crocus and its implementation in SURFEX v7.2, Geosci. Model Dev., 5, 773–791, https://doi.org/10.5194/gmd-5-773-2012, 2012.

Webster, C. and Jonas, T.: Influence of canopy shading and snow coverage on effective albedo in a snow-dominated evergreen needleleaf forest, Remote Sensing of Environment, 214, 48–58, https://doi.org/10.1016/j.rse.2018.05.023, 2018.

Webster, C., Rutter, N., Zahner, F., and Jonas, T.: Measurement of Incoming Radiation below Forest Canopies: A Comparison of Different Radiometer Configurations, Journal of Hydrometeorology, 17, 853–864, https://doi.org/10.1175/JHM-D-15-0125.1, 2016.

Webster, C., Mazzotti, G., Essery, R., and Jonas, T.: Enhancing airborne LiDAR data for improved forest structure representation in shortwave transmission models, Remote Sensing of Environment, 249, 112017, https://doi.org/10.1016/j.rse.2020.112017, 2020.

Webster, C. S.: Measuring and modelling spatiotemporal longwave radiation dynamics in discontinuous forest environments, 2016.

Winstral, A., Jonas, T., and Helbig, N.: Statistical Downscaling of Gridded Wind Speed Data Using Local Topography, Journal of Hydrometeorology, 18, 335–348, https://doi.org/10.1175/JHM-D-16-0054.1, 2017.

Wood, E. F., Roundy, J. K., Troy, T. J., Beek, L. P. H. van, Bierkens, M. F. P., Blyth, E., Roo, A. de, Döll, P., Ek, M., Famiglietti, J., Gochis, D., Giesen, N. van de, Houser, P., Jaffé, P. R., Kollet, S., Lehner, B., Lettenmaier, D. P., Peters-Lidard, C., Sivapalan, M., Sheffield, J., Wade, A., and Whitehead, P.: Hyperresolution global land surface modeling: Meeting a grand challenge for monitoring Earth's terrestrial water, Water Resources Research, 47, https://doi.org/10.1029/2010WR010090, 2011.

Wrzesien, M. L., Kumar, S., Vuyovich, C., Gutmann, E. D., Kim, R. S., Forman, B. A., Durand, M., Raleigh, M. S., Webb, R., and Houser, P.: Development of a "Nature Run" for Observing System Simulation Experiments (OSSEs) for Snow Mission Development, Journal of Hydrometeorology, 23, 351–375, https://doi.org/10.1175/JHM-D-21-0071.1, 2022.

Zheng, Z., Ma, Q., Jin, S., Su, Y., Guo, Q., and Bales, R. C.: Canopy and Terrain Interactions Affecting Snowpack Spatial Patterns in the Sierra Nevada of California, Water Resour. Res., 55, 8721–8739, https://doi.org/10.1029/2018WR023758, 2019.

Supplementary Material for:

Canopy structure, topography and weather are equally important drivers of small-scale snow cover dynamics in sub-alpine forests

Giulia Mazzotti[1,2], Clare Webster[1,3], Louis Quéno[1], Bertrand Cluzet[1], Tobias Jonas[1]

[1]WSL Institute for Snow and Avalanche Research SLF, 7260 Davos Dorf, Switzerland

[2]Univ. Grenoble Alpes, Université de Toulouse, Météo-France, CNRS, CNRM, Centre d'Études de la Neige, 38100 St. Martin d'Hères, France

[3]Department of Geosciences, University of Oslo, 0316 Oslo, Norway

Contents:

S1: Physiographic maps over the full model domain

S2: Canopy structure representation in FSM2

S3: Summary of FSM2 validation at the process-level

S4: Meteorological conditions during the simulation period

S5: Maps of snow cover and energy balance descriptors for WY 2019 over the full model domain

S6: Location of example points within the model domain

S7: Maps of snow cover descriptors for the other simulated WYs

S1: Physiographic maps over the full model domain

To complement the site description in the main article (Section 2.2 and Figure 1), Figure S1.1 reports additional maps of physiographic variables across the model domain, including local canopy cover fraction, elevation, aspect and slope.

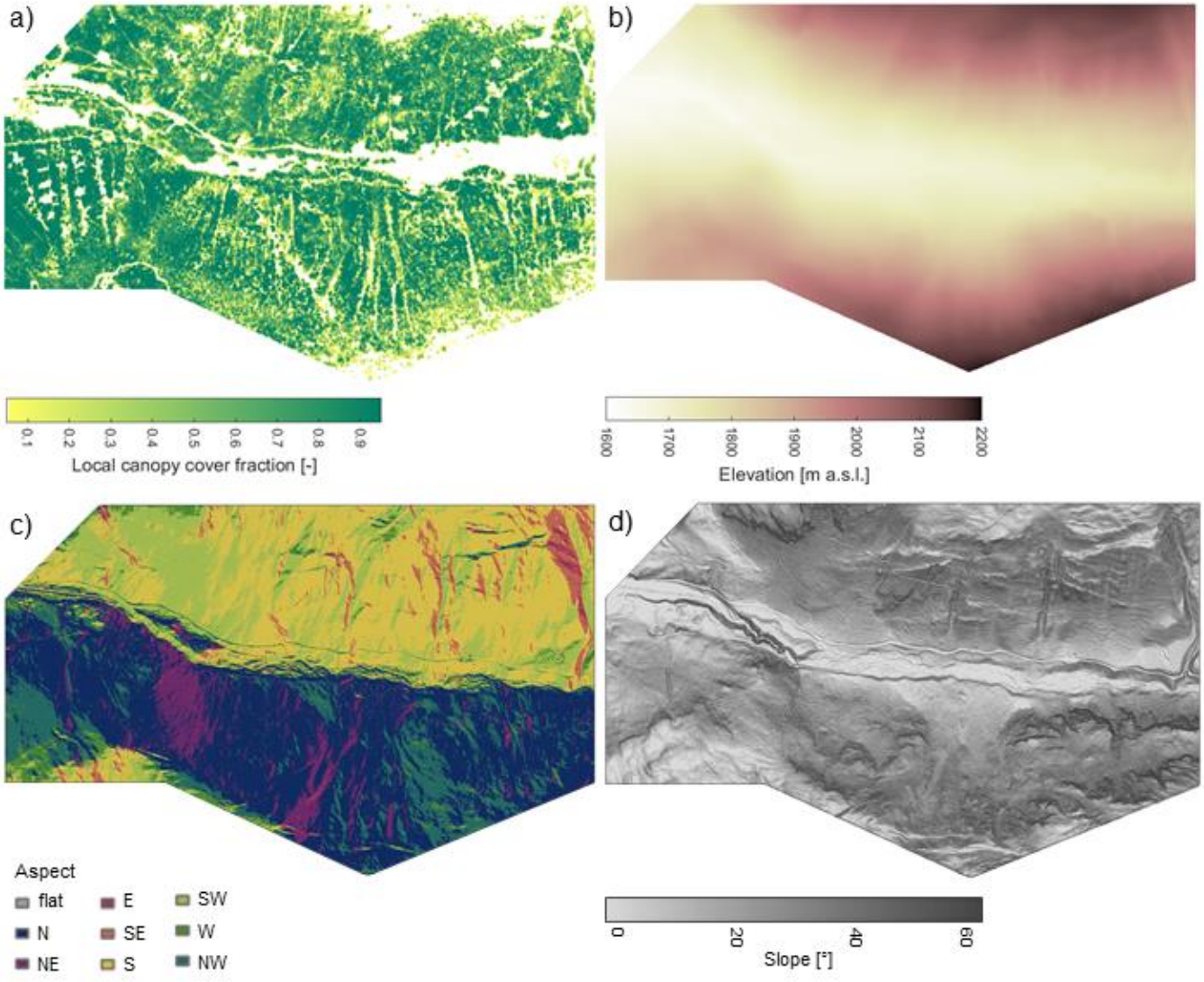

Figure S1.1: Local canopy cover fraction (a), elevation (b), aspect classes (c), and slope (d) across the full model domain.

S2: Canopy structure representation in FSM2

The diversified representation of canopy structure of FSM2 with process-specific canopy metrics constitutes the model's principal asset. With this strategy, FSM2 considers that different canopy-mediated processes are regulated by different and potentially uncorrelated canopy characteristics. A point located in a canopy gap, as example, experiences the interception regime of a very sparse canopy, but may be affected by frequent shading, which implies conditions typical of a dense canopy. These independent and contrasting canopy controls on each of the various processes cannot be reproduced if all processes are parametrized with the same, bulk canopy descriptors. Bulk canopy metrics may thus be suited for intermediate- or coarse-resolution model applications targeting the estimation of spatially averaged fluxes and states, but hyper-resolution approaches that strive to reproduce meter-scale patterns require explicit representation of a wide range of detailed canopy features. The canopy metrics used within FSM2 comprise horizontal, vertical, local, and stand-scale canopy characteristics at each modelled location. Consequently, the canopy's structural diversity is captured even though canopy is represented with a so-called one-layer model. Figure S2.1 illustrates this concept, summarizing the different canopy perspectives, the corresponding metrics, approaches, and data sources used to derive them, and the processes employing them. The schematic complements the mathematical formulation of the process parametrizations provided in the respective model description papers, Essery (2015) and Mazzotti et al. (2020a,b).

Transmission of direct shortwave radiation through the canopy involves a particularly complex interaction with small-scale canopy elements. Because transmissivity is dictated by the presence of canopy elements in the path of the solar beam, it depends on the exact geometric arrangement of the point of interest, the canopy, and the sun, and is thus highly variable in space and time. By accepting transmissivity time series as model input, FSM2 forgoes simplification of the process representation that comes with any parametrization, and instead leverages the benefits of an (external) radiative transfer model that resolves the process explicitly. So far, FSM2.0.3 has been used in tandem with the radiative transfer model HPEval (Jonas et al., 2020), which comprises a traditional approach to compute transmissivity time series at a point based on a high-resolution hemispherical image. The radiative transfer model depicted in the schematic in Figure S2.1 illustrates the HPEval approach. In this study, transmissivity time series are computed following the HPEval methodology based on synthetic hemispherical images derived from LiDAR datasets instead of real ones. The workflow to create these synthetic images, detailed in Webster et al. (2020), integrates canopy segmentation algorithms to identify individual trees in a canopy height model and point cloud enhancing algorithms to densify the point cloud, aimed at mimicking opaque stems and branches. The resulting images feature more realistic and detailed tree shapes than images obtained with unprocessed LiDAR data (see Section S3).

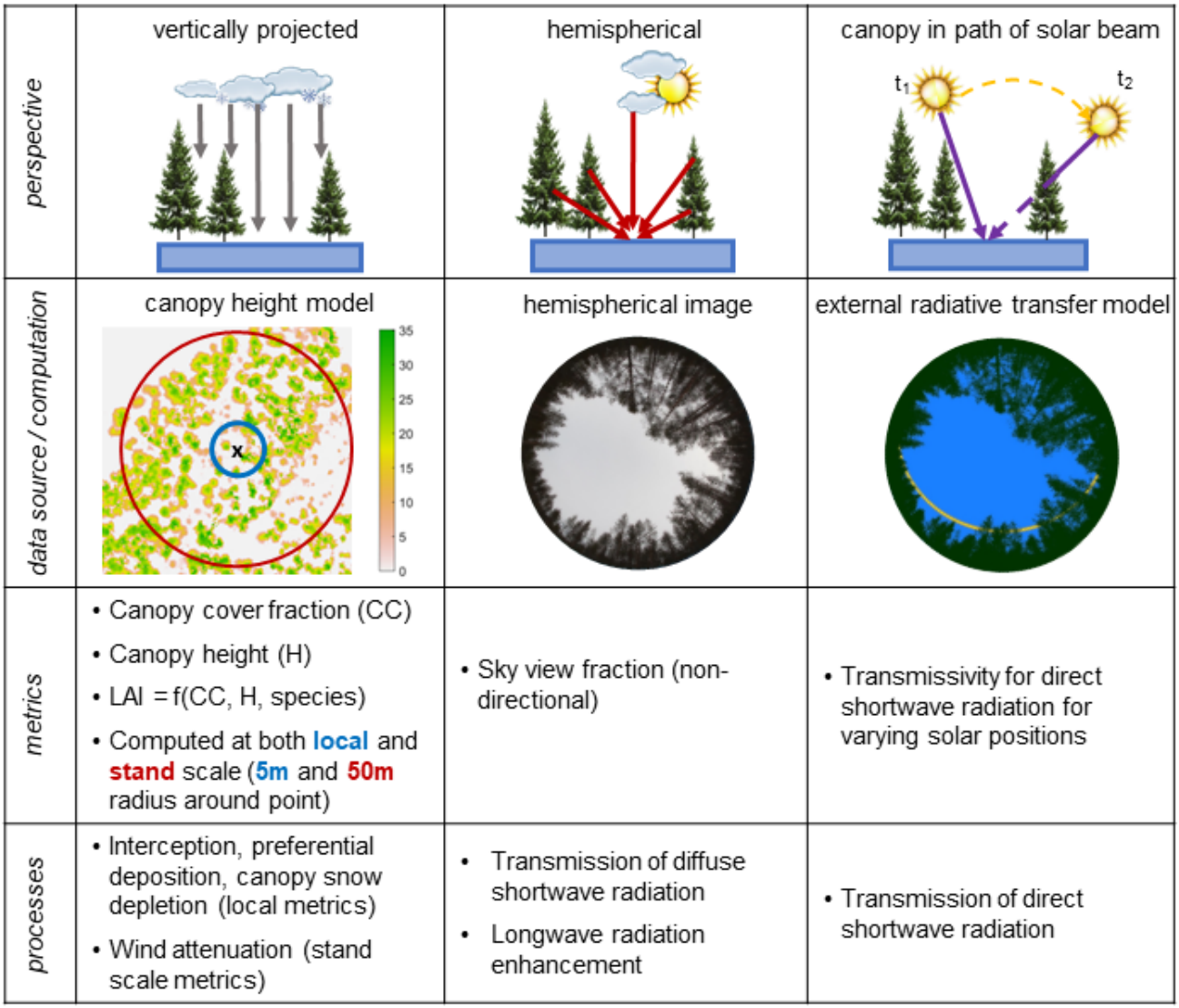

Figure S2.1: Overview of the concepts underlying the canopy structure representation in FSM2: different perspectives, relevant data sources and computation approaches, resulting metrics, and modelled processes that use the respective metrics.

S3: Summary of FSM2 validation at the process level

This study relies on FSM2's capability to accurately simulate the spatio-temporal patterns of individual fluxes and states that constitute forest snow processes, which was extensively tested in a previous study by Mazzotti et al. (2020a). Figure S3.1 reports an example of their validation efforts to illustrate the underlying methodology. Data were acquired with multiple meteorological sensors mounted on a motorized cable car platform (Figure S3.1). Over the course of a winter, the system was deployed along several forest transects of approx. 50 m length each in both Switzerland and Finland. Surveys covered variable canopy structures and forest species, weather conditions, as well as sub-alpine and boreal climates. Observations from the cable car setup were complemented by data from two additional handheld and stationary setups, yielding a dataset with an unprecedented variety of micro-meteorological and snow measurements. FSM2 simulations at high spatial and temporal resolution were directly compared to the acquired datasets. The example in Figure S3.1 features measurements from a full 24-hour cycle along a cable car transect and corresponding FSM2 simulations at 1.5m spacing and 10min temporal resolution. To our knowledge, FSM2 is the only forest snow model to have ever undergone such a rigorous validation.

FSM2's ability to replicate individual fluxes and states and their spatial and temporal variability was quantitatively assessed in terms of transect averages and standard deviations of all measured variables across all available datasets (Figure S3.2). Root means square errors (RMSE) of 23 Wm^{-2} and 4Wm^{-2} resulted for average shortwave and longwave irradiances, respectively, while their standard deviations featured RMSEs of 21Wm^{-2} and 2Wm^{-2}. RMSEs of mean and standard deviation of canopy air space temperatures were 1.6°C and 0.4°C, for snow surface temperatures they amounted to 0.6°C and 0.4°C. Performance metrics all showed substantial improvements relative to the standard land surface model canopy implementation that was used as benchmark in Mazzotti et al. (2020a).

The accuracy of the shortwave radiative transfer calculations in FSM2 is dictated by the accuracy of the external radiative transfer model. Webster et al. (2020) showed that shortwave radiation estimates using synthetic images obtained with the LiDAR enhancing methodology were similar to estimates obtained with real images (Figure S3.3, a-e), and patterns of shadows on the snow surface (f) matched those captured with UAV-imagery (g) with high level of detail.

While plausibility checks as presented in Section 2.3 (main article) are important to ensure model applicability for a specific use case, we believe that quantitative validations at the level of individual fluxes and states such as in Mazzotti et al. (2020a) and summarized here are more conclusive than assessments based on snow extent and depth data alone.

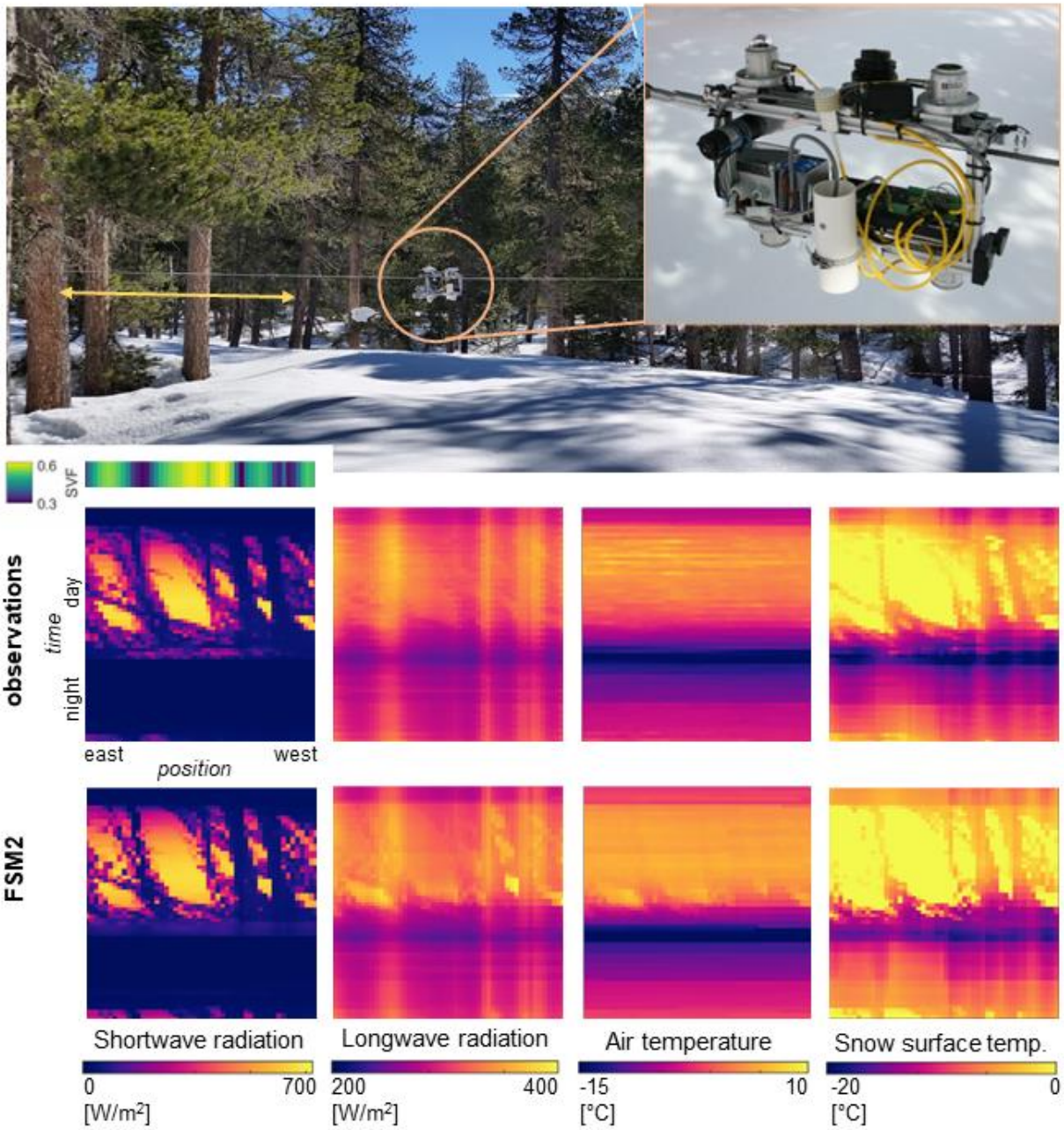

Figure S3.1: The multi-sensor platform in operation along a 50-m cable (yellow arrow) in a pine stand near Davos, Switzerland below variable canopy cover (sky-view fraction, SVF, obtained from hemispherical photographs acquired along the transect). Resulting model validation: observed spatiotemporal variability of measured variables during a 24-h cycle (19. to 20.03.2019) and corresponding FSM2 simulations. The direct comparison between model results and observations is achieved by extracting model output at each point based on the time stamp of the respective observation. Adapted from Mazzotti et al. (2020a), Fig. 1 and 3.

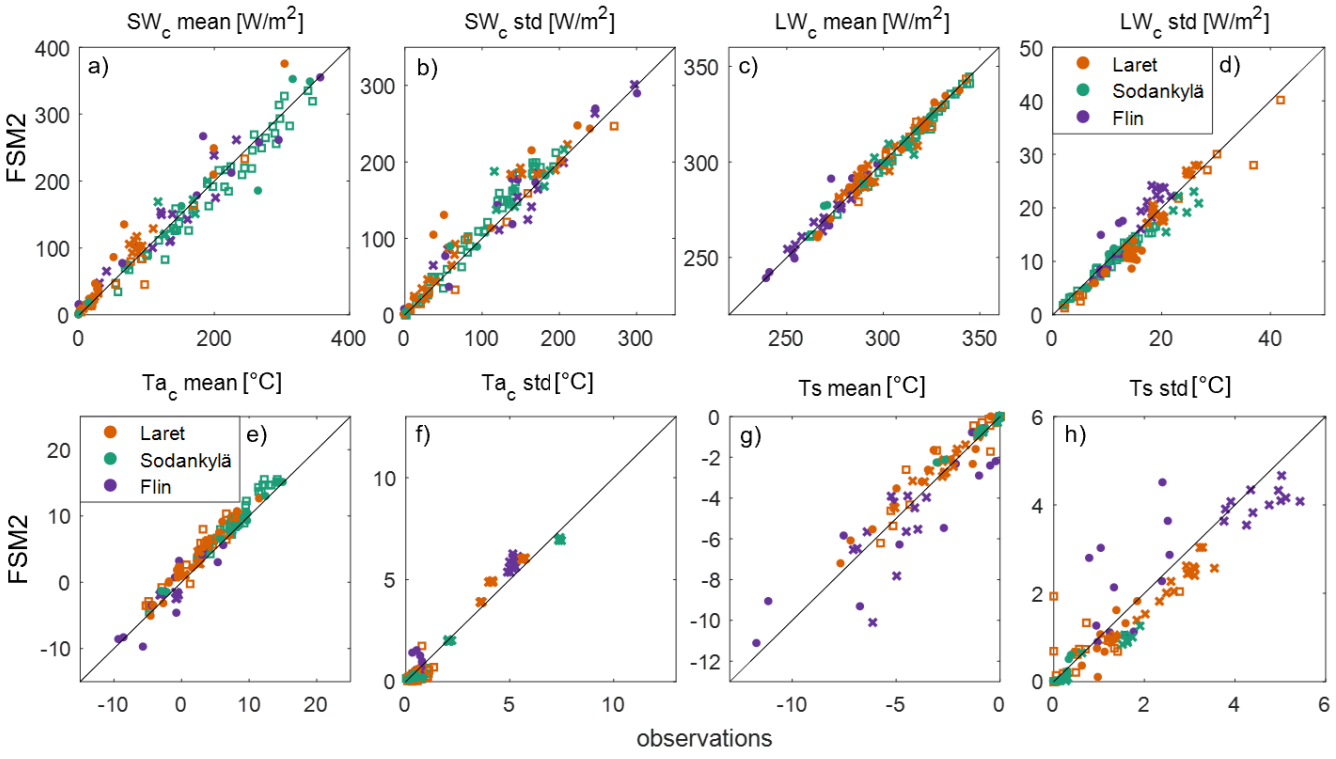

Figure S3.2: Observed vs. modelled averages and standard deviations of subcanopy shortwave (a,b) and longwave (c,d) irradiances, canopy air space (e,f) and snow surface (g,h) temperatures. Data points correspond to temporal averages at point locations (crosses), spatial averages along the cable car transects (dots), and spatial averages over plots surveyed with a handheld setup (squares) at given points in time. Individual colors represent each study area, where Laret and Flin are located in the Eastern Swiss Alps and Sodankylä in sub-arctic Finland. Adapted from Mazzotti et al. (2020a), Figures 5 and 7.

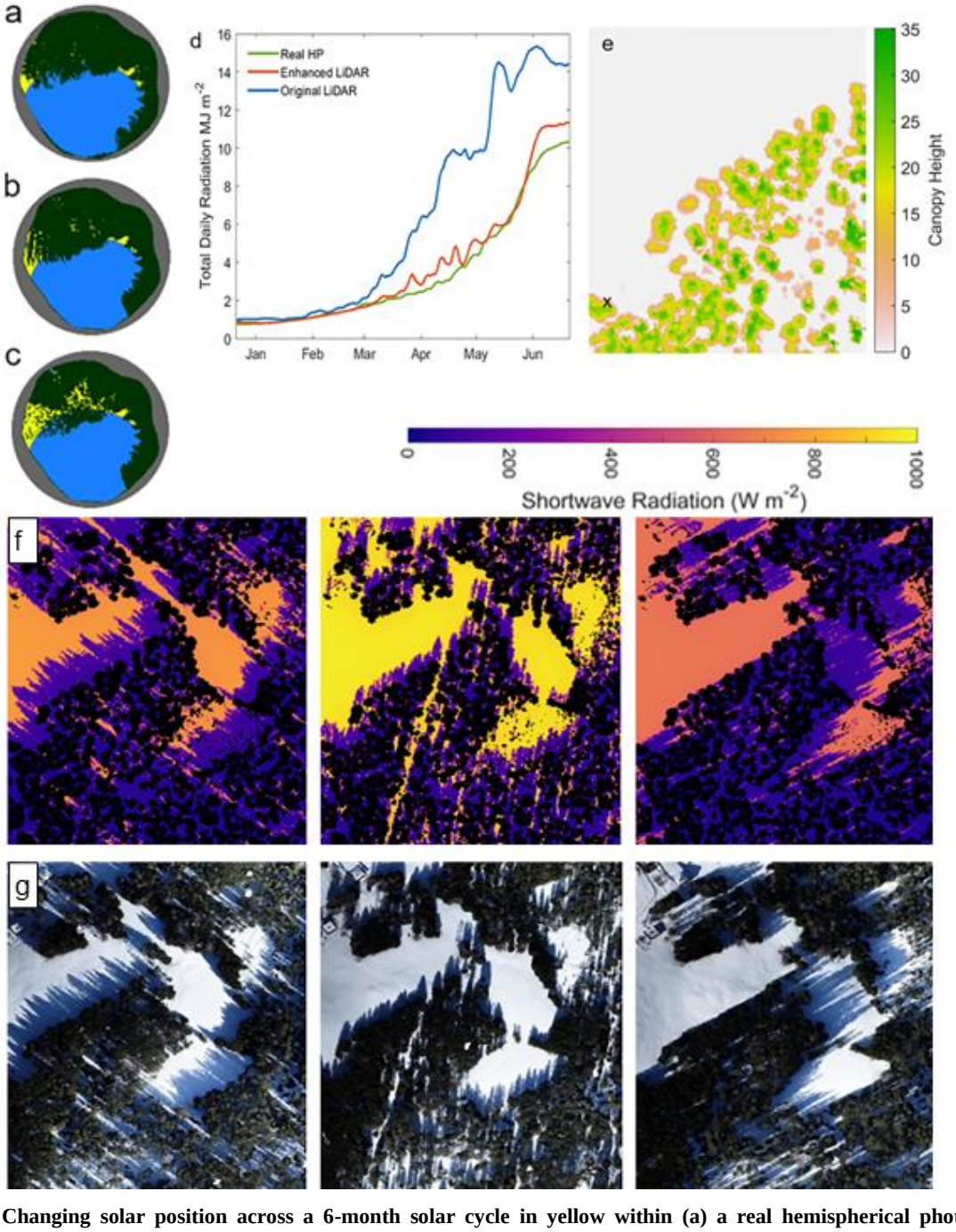

Figure S3.3: Changing solar position across a 6-month solar cycle in yellow within (a) a real hemispherical photograph, (b) synthetic hemispherical images from the enhanced LiDAR and (c) original LiDAR. Modelled total daily radiation across the same period (d) at location X in the canopy height model (e). Comparison of modelled radiation (f) and snow surface shadowing as photographed from a drone (g) at 09:30 (left), 12:30 (center) and 15:30 (right) on 28.03.2019. Adapted from Webster et al. (2020), Fig. 8 and 10.

S4: Meteorological conditions during the simulation period

The following figures provide an overview of meteorological conditions during the six simulated water years to give context to the observed differences in snow cover dynamics outlined in the main article. We focus on the three variables that, as elaborated on in the main article, have the largest potential to cause differences between years: snowfall (affects total accumulation), shortwave radiation, and temperature (affect the timing and strength of melt, as well as whether it is mainly driven by short- or longwave radiation contributions). The left panel of Figure S4.1 reports weekly snowfall sums between the beginning of November and June, which represent the earliest and latest yearly median of the start of snow cover period and snow disappearance date. Some marked differences in how the precipitation is distributed throughout the snow season can be observed. The right panel of Figure S4.1 shows cumulative snowfall between the median start of snow cover and snow disappearance dates of each specific year. This visualization evidences the substantial differences in timing and length of snow cover period and total snowfall between the years, with WY2016 (lowest accumulation) amounting to only half of total snowfall of WY 2019 (highest accumulation).

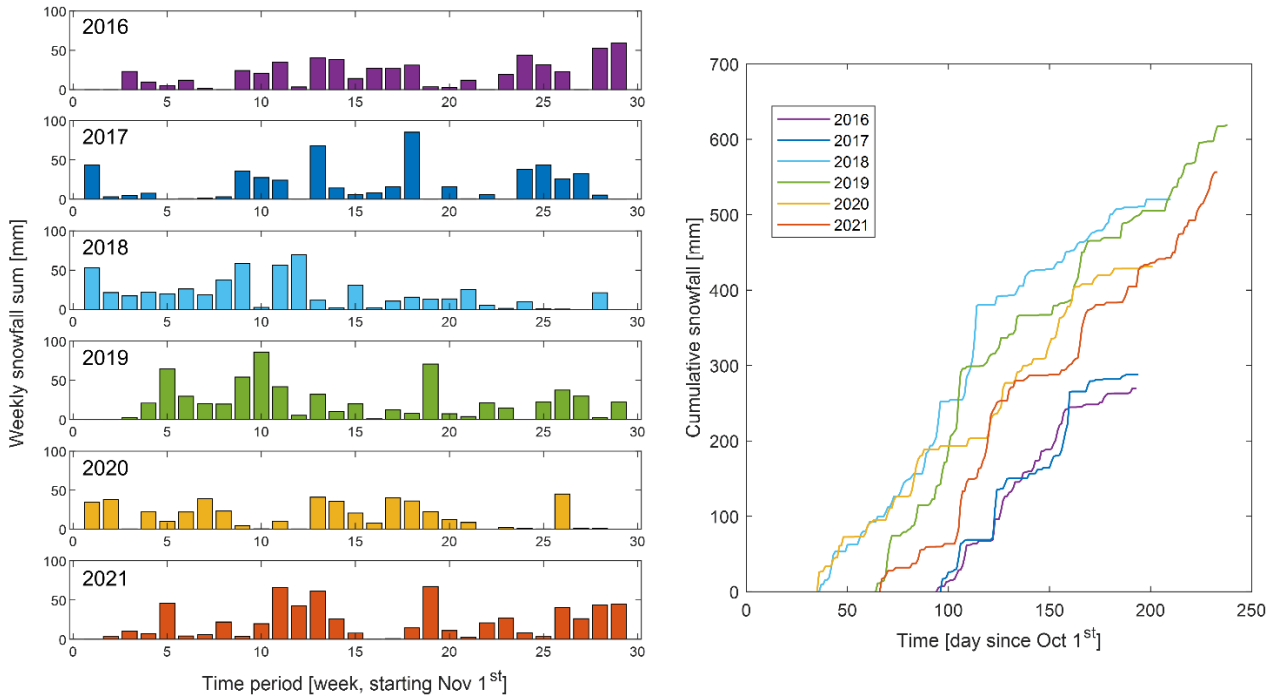

Figure S4.1: Weekly snowfall during the six modelled winters between November and June (left) and cumulative snowfall over the median snow cover duration period of the respective year (right).

Figure S4.2 contrasts shortwave radiation (left) and air temperatures (right) during the six simulated winters, with the upper row showing weekly values and the lower row the weekly deviation from the six-year average. While no year is clearly above or below average for any of the two variables for the entire season, some marked deviations from the averages can be detected in these plots, for instance the relatively warm period in the middle of the 2020 winter.

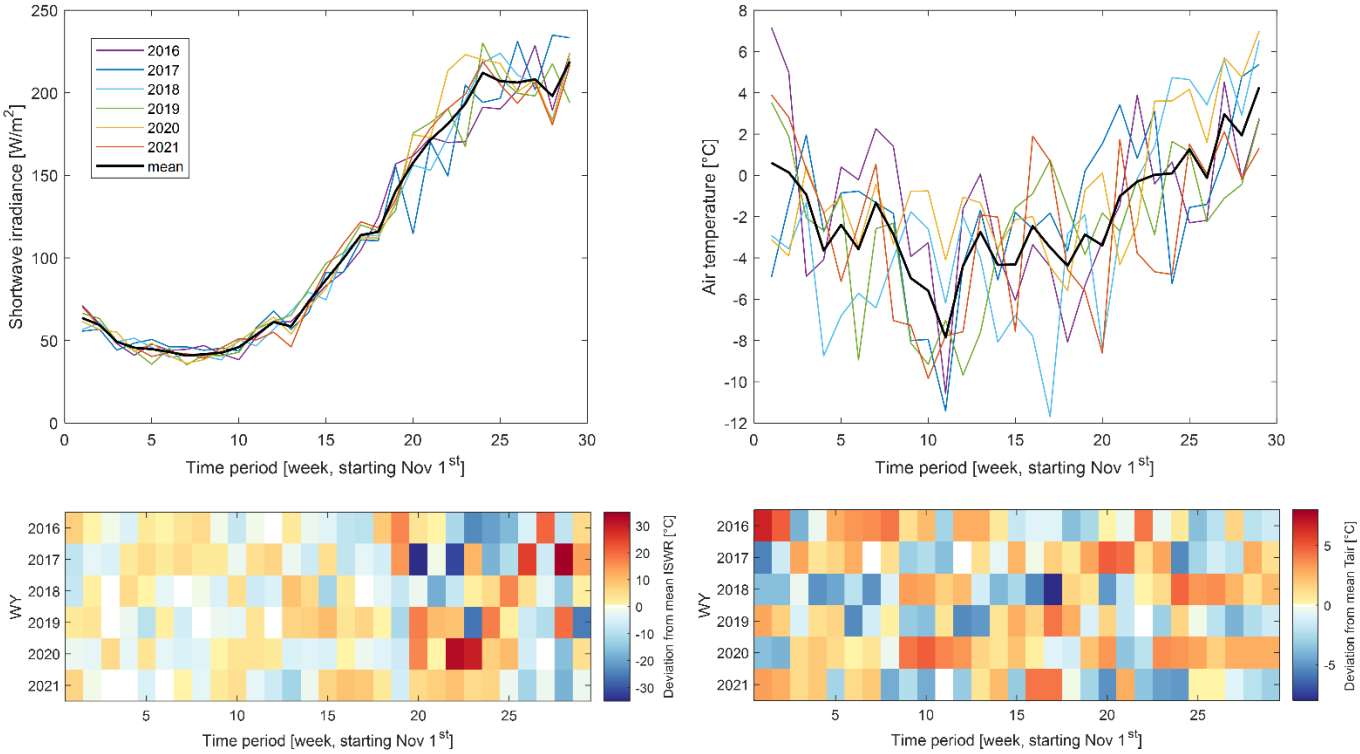

Figure S4.2: Incoming shortwave radiation (left) and air temperature (top right) of the six simulated winters, and deviation from mean (lower row) for the same variables.

S5: Maps of snow cover and energy balance descriptors for WY2019 over the full model domain

While some figures in the main article include maps of a subdomain of the model domain to illustrate patterns of snow cover descriptors and energy fluxes, here we add the corresponding maps for the full model domain for interested readers. Figure S5.1 reports peak SWE, ablation rate, day of peak SWE and snow disappearance day for WY 2019, corresponding to Figure 5 of the main article.

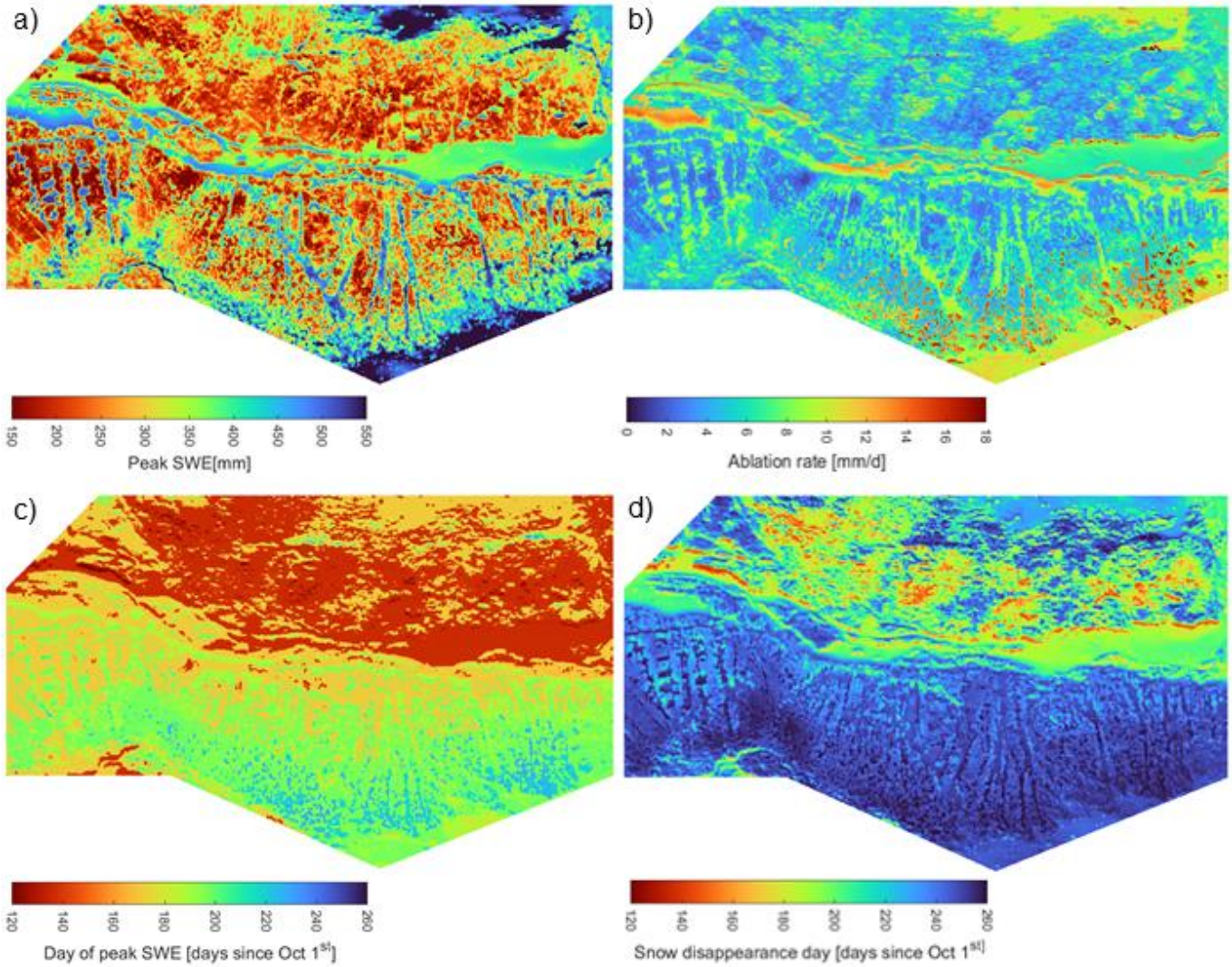

Figure S5.1: Peak SWE (a), ablation rate (b), day of peak SWE (c) and snow disappearance day (d) in WY 2019.

Figure S5.2 shows average incoming irradiances and early melt between mid-January and end of February 2019, analogous to Figure 7 of the main article. Note the addition of incoming longwave radiation which further underpins the statement that all-wave irradiance patterns are largely determined by patterns of incoming shortwave radiation.

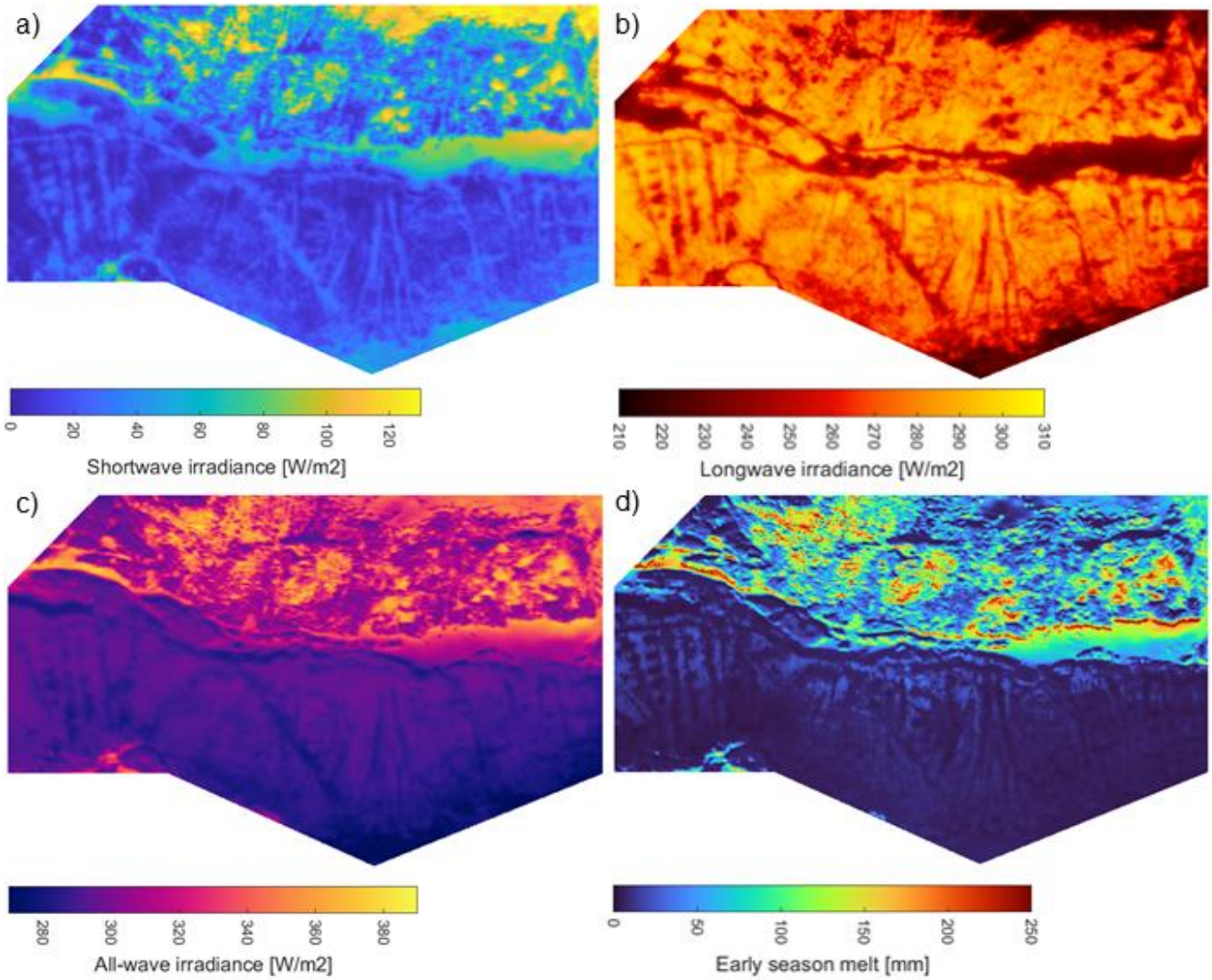

Figure S5.2: Average incoming short (a) and longwave (b) radiation, all-wave radiation (c) and snow melt (d) between mid-January and end of February 2019.

Figure S5.3 includes average patterns of the individual surface energy balance components (net short- and longwave radiation, sensible and latent heat) as well as net surface energy flux computed as the sum of the four. Maps shown are for the second half of February 2019, analogous to the upper part of Figure 8 in the main article.

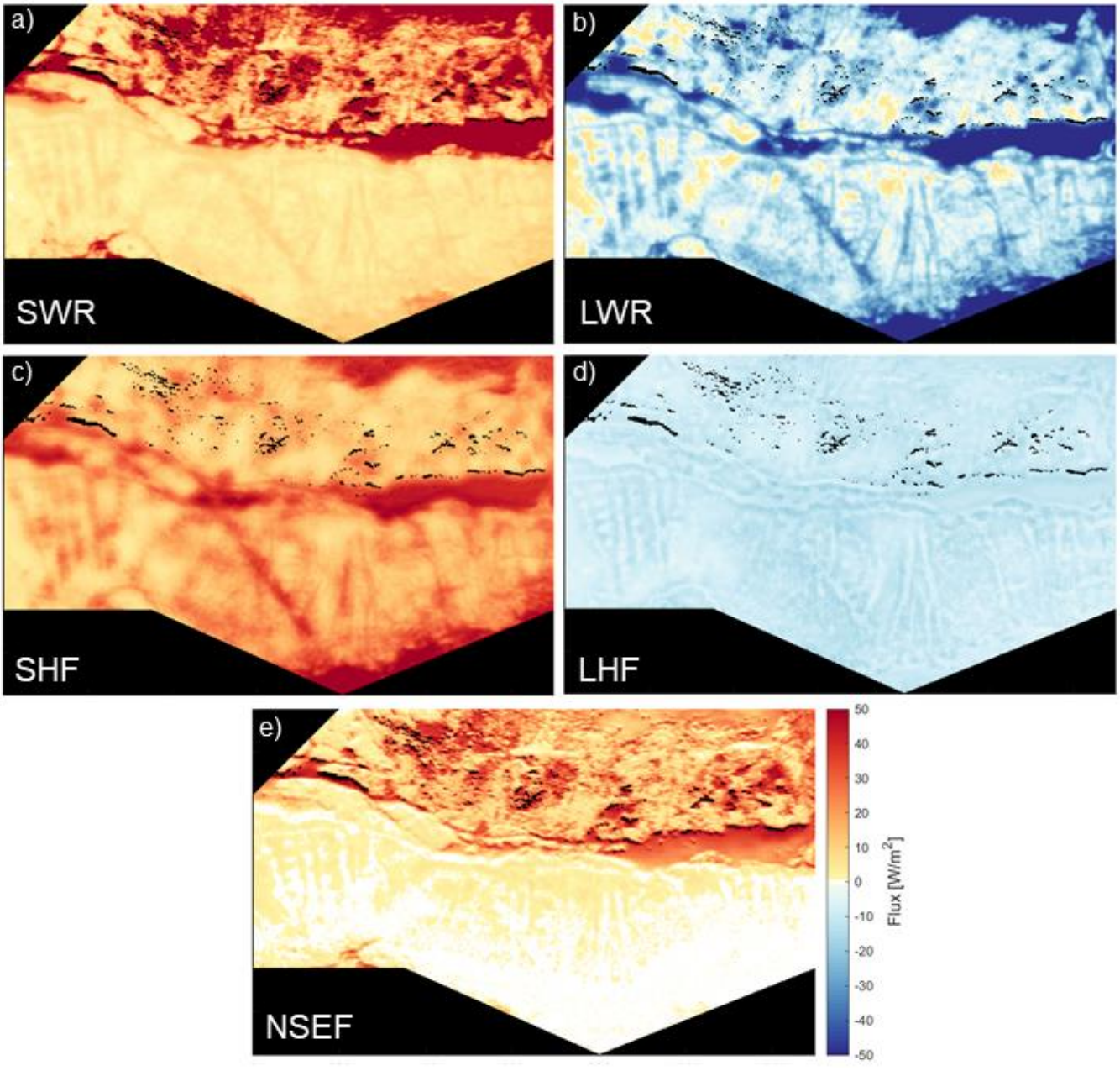

Figure S5.3: Individual surface energy components (net short- and longwave radiation, SWR (a) and LWR (b), as well as sensible and latent heat fluxes, SHF (c) and LHF (d)) and net surface energy flux (NSEF, e) computed as sum of the four, for the second half of February 2019.

S6: Location of example points within the model domain

The location of example points used for the analysis of snow evolution and energy balance partitioning pathways presented in Section 3.3 and 3.5 are shown in Figure S6.1. In Section 3.3, points were chosen to cover the entire range of canopy structures and topographic locations (Figure S6.1b, corresponding to points shown in Figure 6 of the main article). In Section 3.5, we focused our analysis on points located at the south-exposed slope and sparse canopy or small gaps to explore differences between years (Figure S6.1c, corresponding to points shown in Figure 10 of the main article).

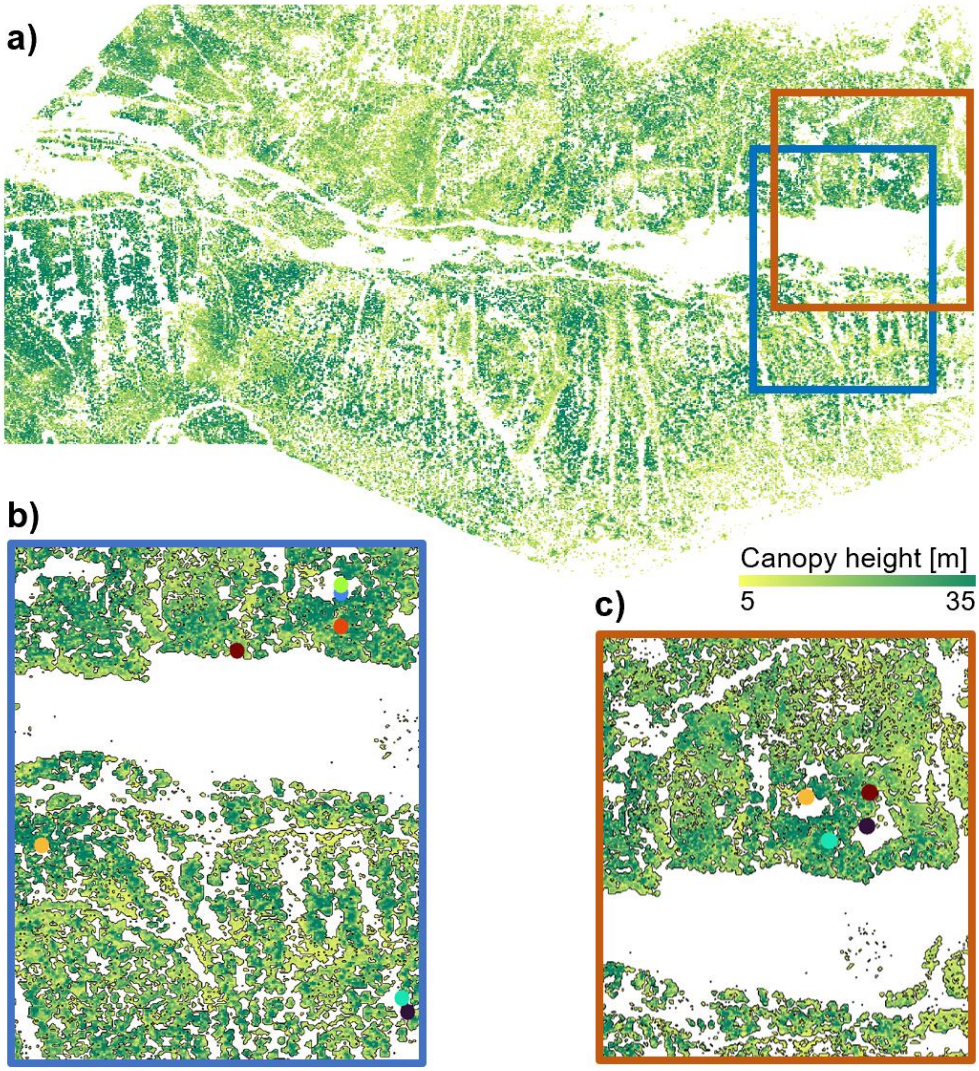

Figure S6.1: Locations of example points. Overview (a), points presented in Section 3.3 / Figure 6 of the main article (b), and points used in Section 3.5 / Figure 10 of the main article. Colours marking individual points match the colour code of the figures in the main article.

S7: Maps of snow cover descriptors for the other simulated WYs

In Section S5, we presented full-domain maps of snow cover descriptors for WY 2019, which is used as main example throughout the article. To complement Figure S5.1, Figures S7.1 to S7.5 report snow cover descriptors for all other simulated WYs. These figures provide an additional visual impression of the between-year consistencies and differences of these snow metrics. Moreover, it should be noted that correlation coefficients presented in Section 3.2 of the main article rely on these data.

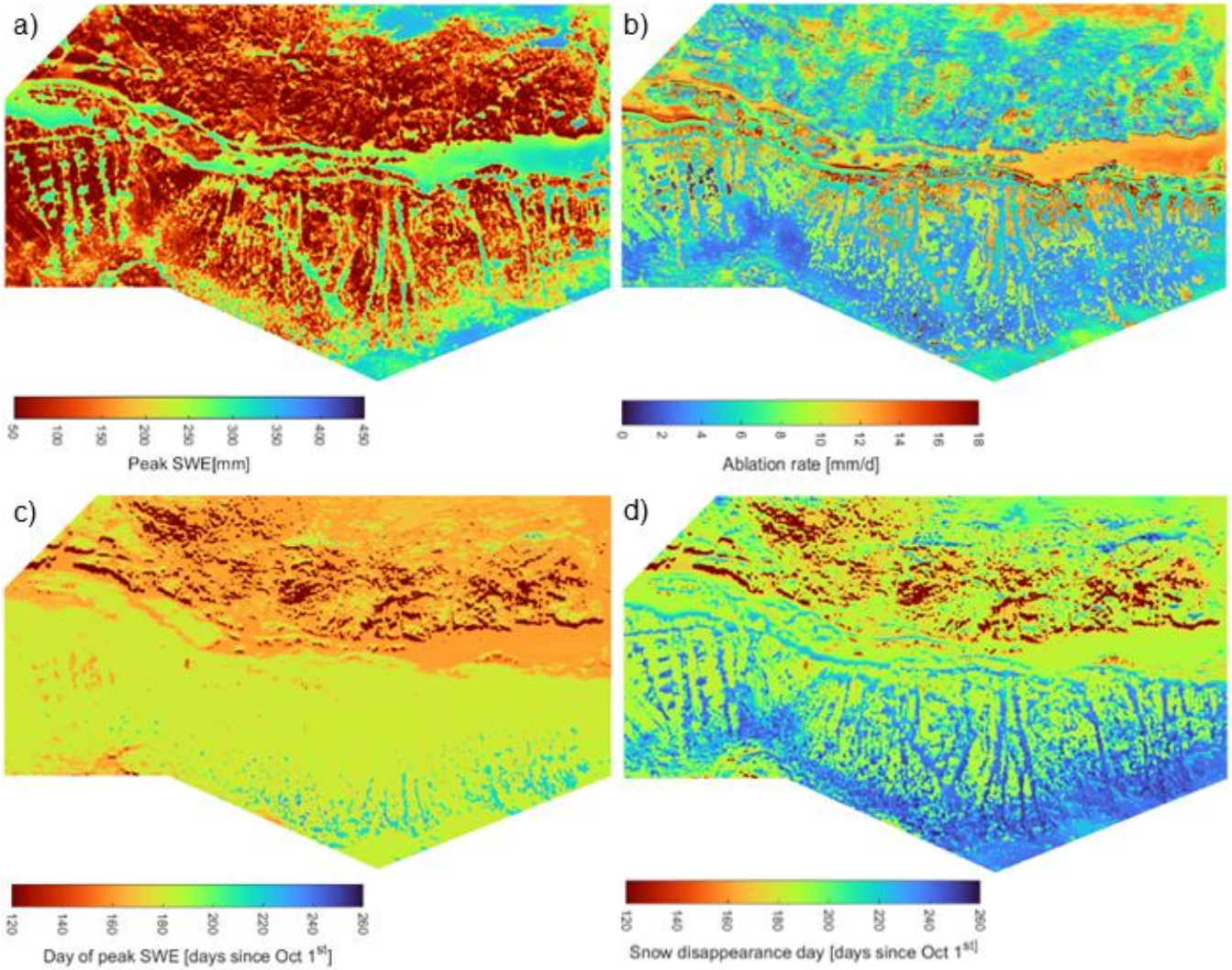

Figure S7.1: Peak SWE (a), ablation rate (b), day of peak SWE (c) and snow disappearance day (d) in WY 2016.

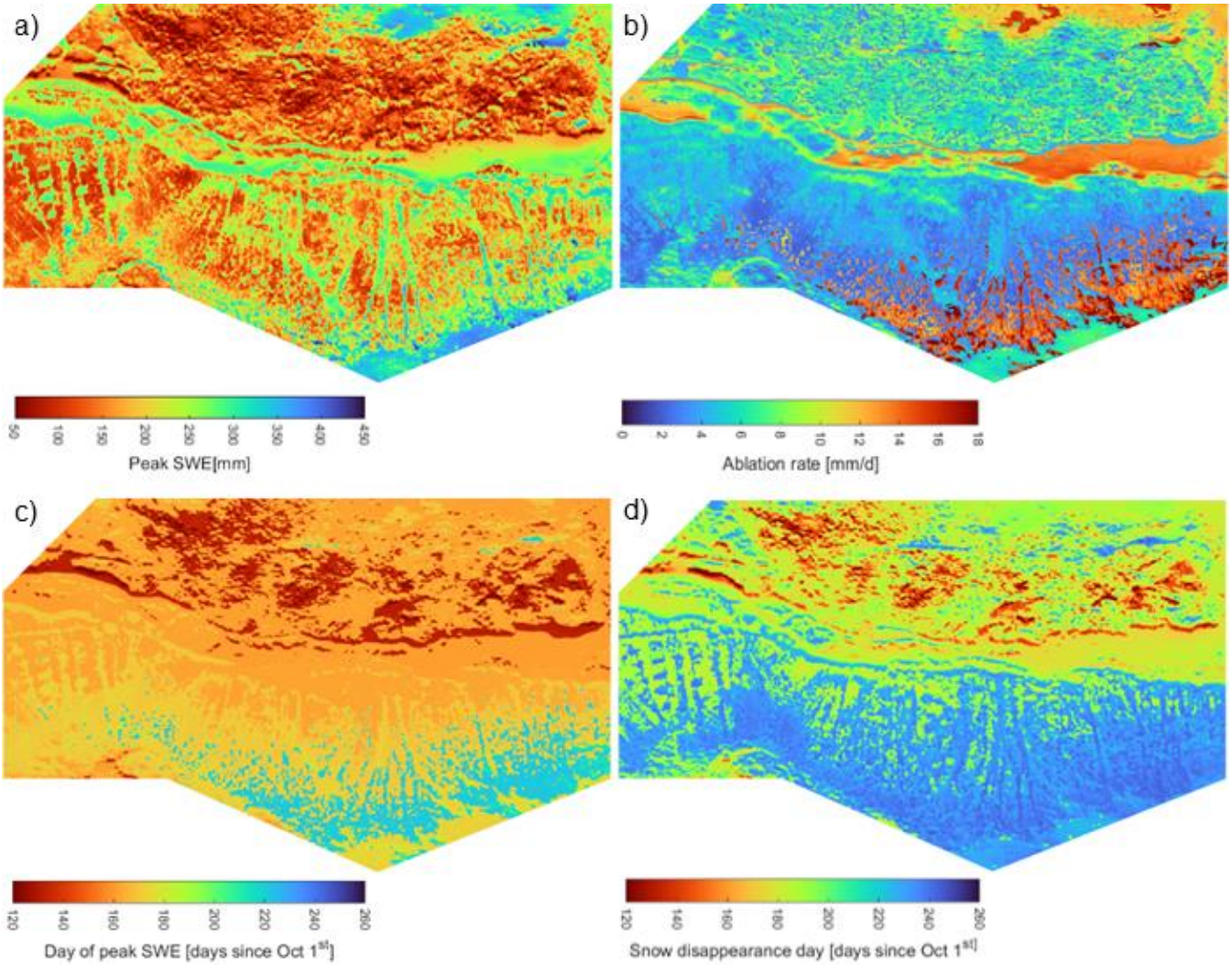

Figure S7.2: Peak SWE (a), ablation rate (b), day of peak SWE (c) and snow disappearance day (d) in WY 2017.

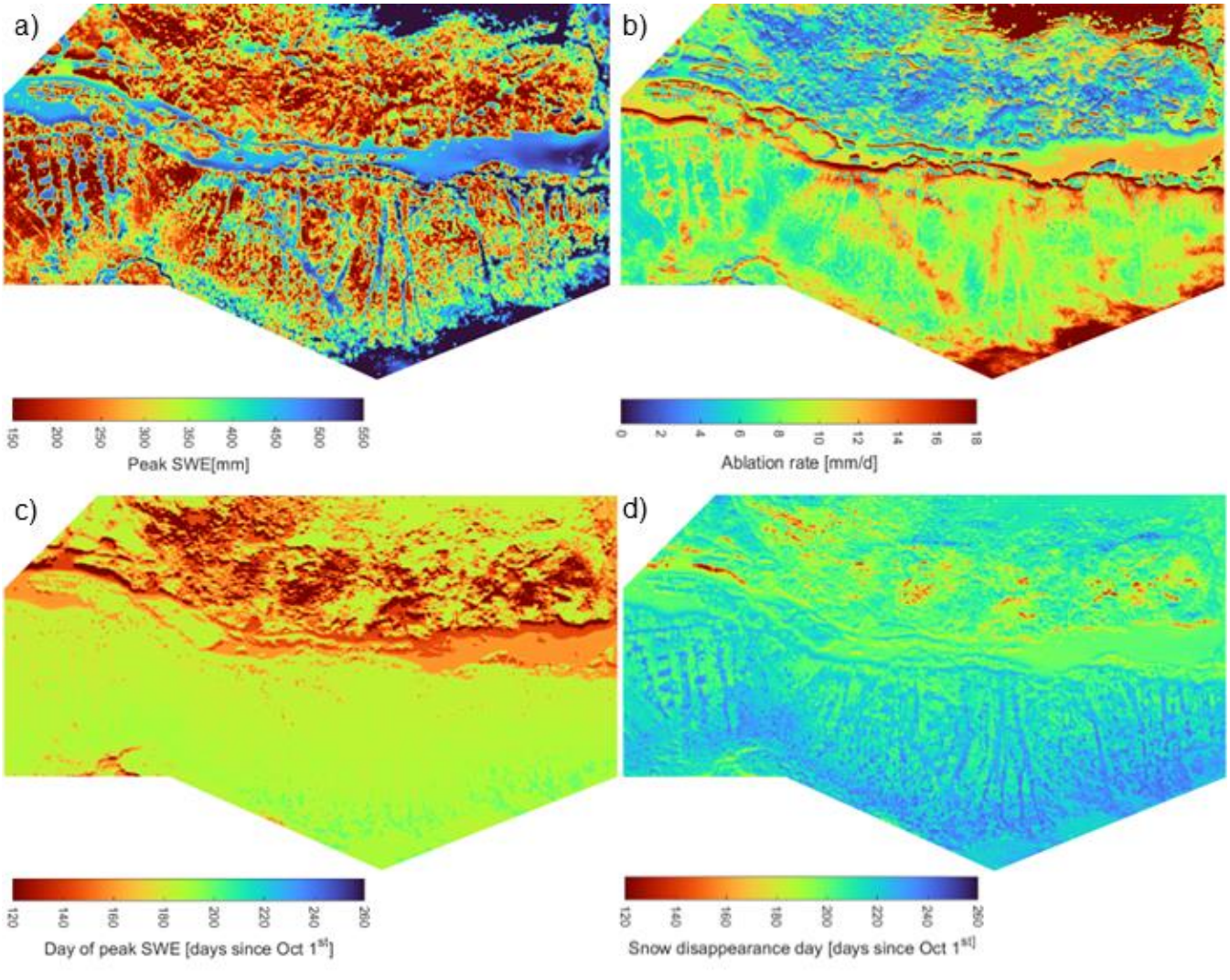

Figure S7.3: Peak SWE (a), ablation rate (b), day of peak SWE (c) and snow disappearance day (d) in WY 2018.

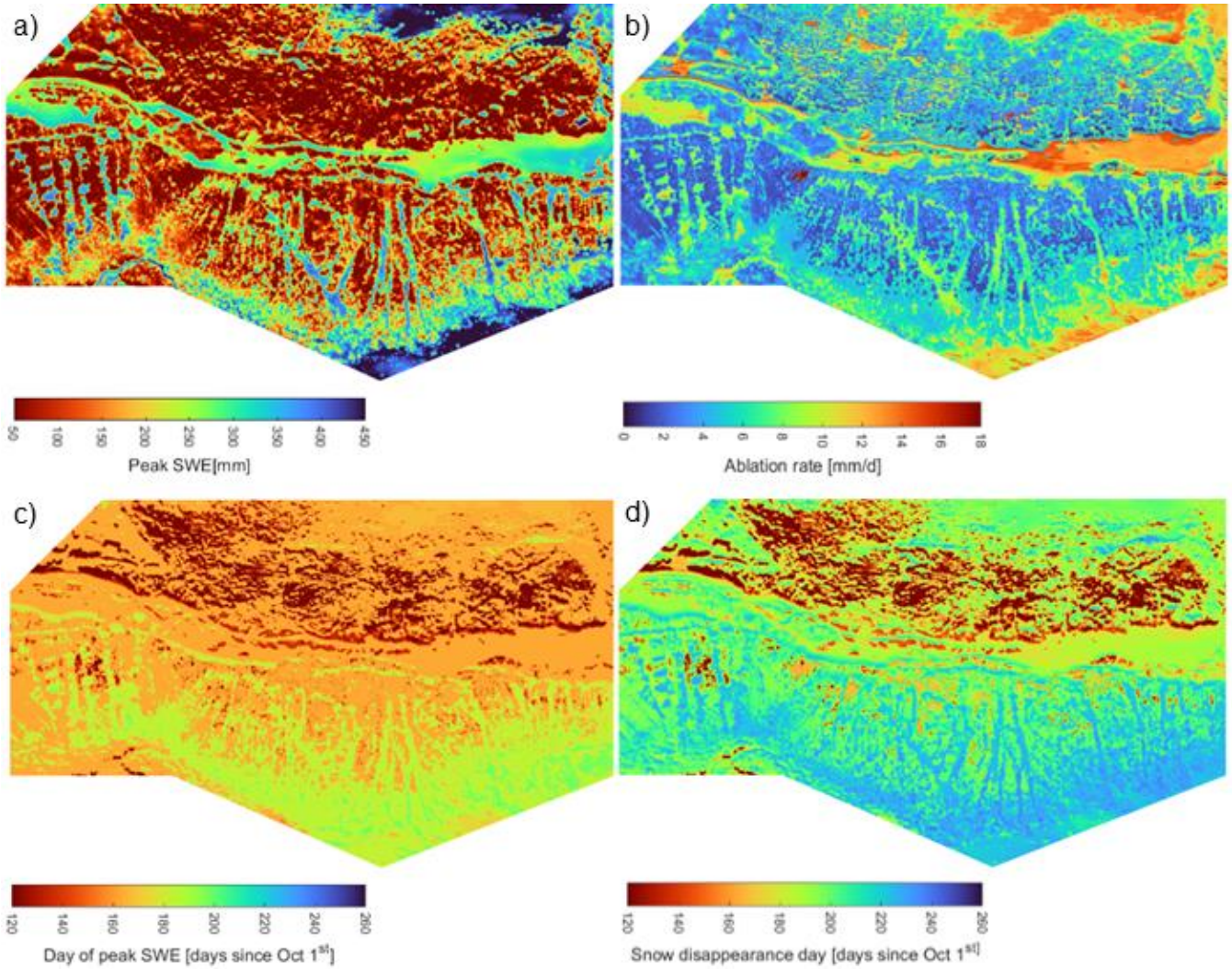

Figure S7.4: Peak SWE (a), ablation rate (b), day of peak SWE (c) and snow disappearance day (d) in WY 2020.

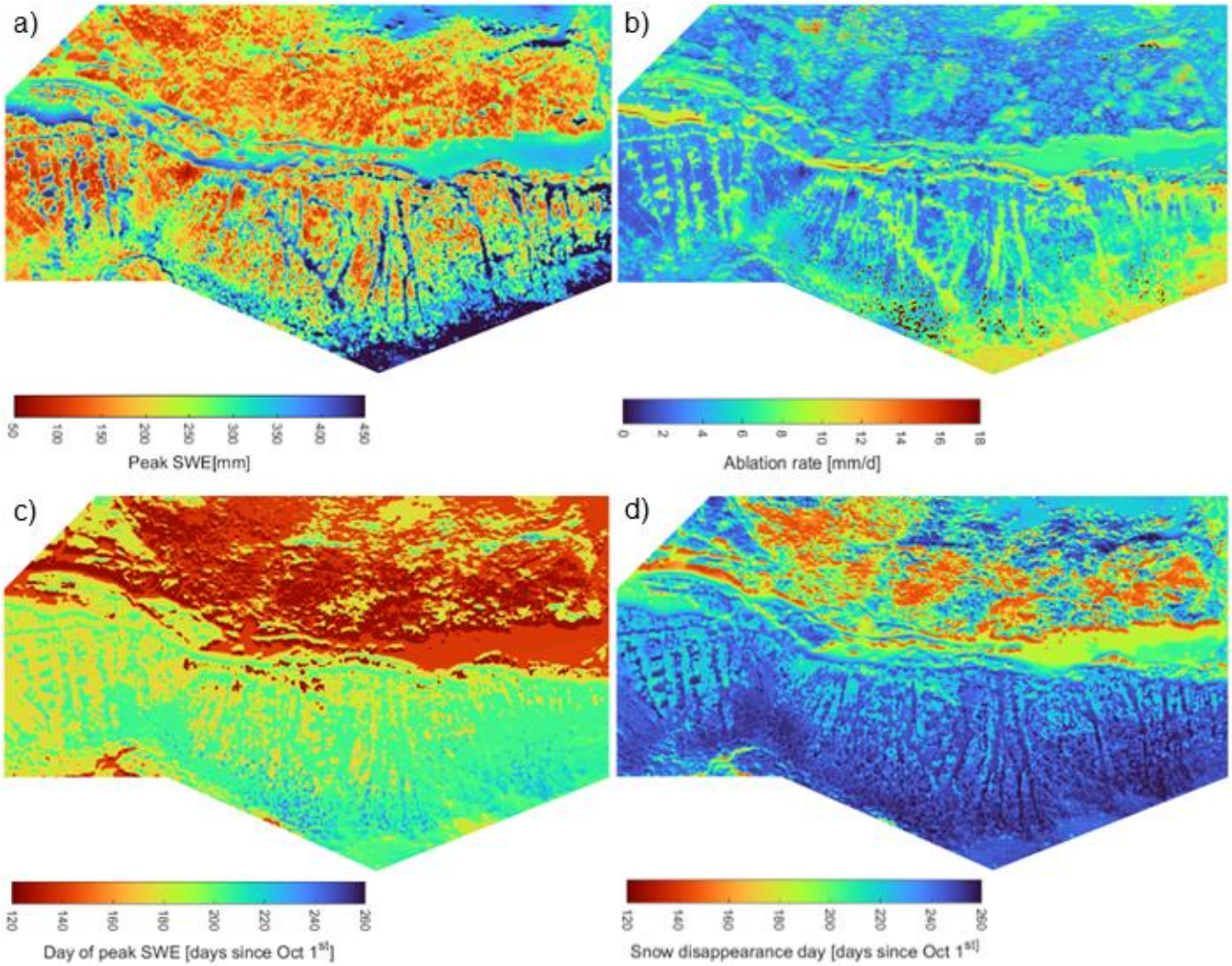

Figure S7.5: Peak SWE (a), ablation rate (b), day of peak SWE (c) and snow disappearance day (d) in WY 2021.

References:

Essery, R.: A factorial snowpack model (FSM 1.0), Geoscientific Model Development, 8, 3867–3876, https://doi.org/10.5194/gmd-8-3867-2015, 2015.

Jonas, T., Webster, C., Mazzotti, G., and Malle, J.: HPEval: A canopy shortwave radiation transmission model using high-resolution hemispherical images, Agricultural and Forest Meteorology, 284, 107903, https://doi.org/10.1016/j.agrformet.2020.107903, 2020.

Mazzotti, G., Essery, R., Webster, C., Malle, J., and Jonas, T.: Process-Level Evaluation of a Hyper-Resolution Forest Snow Model Using Distributed Multisensor Observations, Water Resources Research, 56, e2020WR027572, https://doi.org/10.1029/2020WR027572, 2020a.

Mazzotti, G., Essery, R., Moeser, C. D., and Jonas, T.: Resolving Small-Scale Forest Snow Patterns Using an Energy Balance Snow Model With a One-Layer Canopy, Water Resources Research, 56, e2019WR026129, https://doi.org/10.1029/2019WR026129, 2020b.

Webster, C., Mazzotti, G., Essery, R., and Jonas, T.: Enhancing airborne LiDAR data for improved forest structure representation in shortwave transmission models, Remote Sensing of Environment, 249, 112017, https://doi.org/10.1016/j.rse.2020.112017, 2020.